NIST Special Publication 260
NIST SP 260-242

Certification of Standard Reference Material® 2232a

Indium for DSC Temperature and Enthalpy Calibration

Tara J. Fortin
Tobias K. Herman
Amanda A. Koepke
Jolene D. Splett

This publication is available free of charge from:
https://doi.org/10.6028/NIST.SP.260-242

NIST NATIONAL INSTITUTE OF STANDARDS AND TECHNOLOGY
U.S. DEPARTMENT OF COMMERCE

NIST Special Publication 260
NIST SP 260-242

Certification of Standard Reference Material® 2232a

Indium for DSC Temperature and Enthalpy Calibration

Tara J. Fortin
Applied Chemicals and Materials Division
Material Measurement Laboratory

Tobias K. Herman
Sensor Science Division
Physical Measurement Laboratory

Amanda A. Koepke
Jolene D. Splett*
Statistical Engineering Division
Information Technology Laboratory

**Former NIST employee; all work for this publication was done while at NIST.*

This publication is available free of charge from:
https://doi.org/10.6028/NIST.SP.260-242

September 2024

U.S. Department of Commerce
Gina M. Raimondo, Secretary

National Institute of Standards and Technology
Laurie E. Locascio, NIST Director and Under Secretary of Commerce for Standards and Technology

NIST SP 260-242
September 2024

Publication History
Approved by the NIST Editorial Review Board on 2023-10-25

How to Cite this NIST Technical Series Publication
Fortin TJ, Herman TK, Koepke AA, Splett JD (2024) Certification of Standard Reference Material® 2232a: Indium for DSC Temperature and Enthalpy Calibration. (National Institute of Standards and Technology, Gaithersburg, MD), NIST Special Publication 260 (SP) NIST SP 260-242. https://doi.org/10.6028/NIST.SP.260-242

Author ORCID iDs
Tara J. Fortin: 0000-0001-6150-8930
Tobias K. Herman: 0000-0003-4296-6957
Amanda A. Koepke: 0000-0001-9515-0383

Abstract

A new Standard Reference Material® (SRM®), designated SRM 2232a, has been certified for the temperature and enthalpy calibration of differential scanning calorimeters (DSCs). This is a replacement for the previously sold-out version, SRM 2232. SRM 2232a was sourced from a single lot of high-purity (≥ 99.99999% metals basis, by mass) indium. The melting point of SRM 2232a has been certified to be equal to (156.5985 ± 0.0003) °C using a fixed-point cell and direct comparisons with the NIST laboratory reference cell that constitutes NIST's primary realization of the indium freezing point. The enthalpy of fusion of SRM 2232a has been certified to be equal to (28.58 ± 0.17) $J \cdot g^{-1}$ via DSC measurements using an instrument calibrated with certified reference materials obtained from another national metrology institute. This document provides all relevant measurement and analysis details for the certification of SRM 2232a.

Keywords

Calibration; Differential scanning calorimetry; Differential thermal analyzers; Enthalpy of fusion; Indium; Melting temperature.

Table of Contents

List of Tables

List of Figures

Acknowledgments

The authors thank our NIST colleagues Dr. Michal Chojnacky, Bethany Rodman, and Sam Smith for their contributions to the indium fixed-point cell construction, temperature measurements data collection, and the fixed-point cell schematic, respectively.

1. Introduction

Differential Scanning Calorimeters (DSCs) are regularly used in numerous applications including, but not limited to, materials characterization, the evaluation of phase diagrams, purity determinations, kinetic investigations, and heat capacity measurements. DSCs have largely replaced classical precision calorimeters, such as adiabatic calorimeters, because they require smaller sample volumes, less time, and less specialized expertise to run. However, since DSC is not an absolute measurement technique, calibration is essential to ensure the accuracy of measured temperature, enthalpy, and heat capacity. Over the years, NIST has offered several certified Standard Reference Materials® (SRMs®) to support high-quality calibrations for DSC (e.g., SRM 720 Sapphire, SRM 2220 Tin, SRM 2221a Zinc, SRM 2234 Gallium, SRM 2235 Bismuth, and SRM 2225 Mercury). The most popular of these, SRM 2232 Indium DSC Calibration Standard, sold out of its existing inventory in 2017 yet continues to attract interest.

To meet this persistent need, we have developed a replacement certified indium standard for the calibration of DSCs. The new standard reference material is designated as SRM 2232a and the certified melting temperature (t_m) and enthalpy of fusion (ΔH_{fus}) values are shown in Table 1, along with the associated expanded uncertainties.

Table 1. SRM 2232a Certified Melting Temperature (t_m) and Enthalpy of Fusion (ΔH_{fus}) Values[a] with Expanded[b] Uncertainties.

t_m	=	(156.5985 ± 0.0003) °C
ΔH_{fus}	=	(28.58 ± 0.17) J·g^{-1}

[a]At thermal equilibrium (i.e., zero heating rate).
[b]Uncertainty interval with 95% level of confidence (k = 2 and k = 1.93, respectively).

A unit of SRM 2232a consists of an approximately 1 g ingot sealed in plastic under an inert atmosphere and all ingots were sourced from a single lot of high-purity (≥ 99.99999% metals basis, by mass) indium. The certification of SRM 2232a followed the same general procedures as were utilized during the certification of SRM 2232 [1] but with a few key improvements implemented to comply with evolving requirements. Certification of the melting temperature employed a fixed-point cell constructed from randomly selected SRM 2232a samples and included the evaluation of freezing and melting curves, as well as direct comparison with the laboratory reference cell used to realize the indium freezing point in the NIST Standard Platinum Resistance Thermometer Calibration Laboratory (SPRTCL). Determination of the enthalpy of fusion employed DSC measurements on 15 samples taken from seven randomly selected ingots of SRM 2232a. The DSC used for these measurements was calibrated using certified reference materials procured from the national metrology institute of Germany

(Physikalisch-Technische Bundesanstalt (PTB)).[1] Details of the materials and measurement methods employed, as well as the associated uncertainty analyses, are provided in the subsequent text.

[1] Certain equipment, instruments, software, or materials, commercial or non-commercial, are identified in this paper in order to specify the experimental procedure adequately. Such identification does not imply recommendation or endorsement of any product or service by NIST, nor does it imply that the materials or equipment identified are necessarily the best available for the purpose.

2. Materials and Methods

2.1. High-Purity Indium

A 2.5 kg lot of high-purity (99.99999% metals basis, by mass) indium (lot # 135139138114-400) was purchased from Merelex Corporation, Los Angeles, CA. The material was packaged as ~ 1 g ingots sealed in plastic under an inert environment. The supplier's Glow Discharge Mass Spectrometry (GDMS) analysis results indicate a total impurity (on a metals basis) of approximately 0.1 $\mu g \cdot g^{-1}$ (i.e., parts per million, or ppm), primarily from Fe (0.06 $\mu g \cdot g^{-1}$), Pb (0.02 $\mu g \cdot g^{-1}$), Ca (0.01 $\mu g \cdot g^{-1}$), Ni (0.01 $\mu g \cdot g^{-1}$), and Sb (0.008 $\mu g \cdot g^{-1}$) (see Fig. A.1.1 of Appendix A.1). At our request, the supplier also provided GDMS analysis results from an independent lab (EAG Laboratories, Shanghai, China); these results confirmed a purity of 99.999989% (metals basis, by mass) (see Fig. A.1.2 of Appendix A.1).

In an effort to independently verify sample purity, as well as to check lot homogeneity, samples taken from six of the seven ingots used for enthalpy of fusion measurements (labelled "A" – "F") were sent to the National Research Council of Canada (NRC Canada, Ottawa, Ontario, Canada) for GDMS analysis. Unfortunately, size limitations of the available indium ingots restricted the analysis to standard detection levels, which resulted in fewer quantified elements than the supplier's analysis produced. Even at the lower detection limit, the NRC Canada results indicate purities of $\geq$ 99.99999% (metals basis, by mass) for all six samples (see Figs. A.1.3 – A.1.8 of Appendix A.1). Additionally, no statistically significant differences are observed between the six samples, indicating lot homogeneity.

2.2. Determination of Melting Temperature

One of the freezing points required to realize the International Temperature Scale of 1990 (ITS-90) is that of indium (156.5985 °C) [2, 3]. This freezing point is determined by means of a thermometric fixed-point cell containing high-purity (> 99.9999%) indium metal, which is used for the calibration of standard platinum resistance thermometers (SPRTs).

To certify the melting temperature, t_m, for SRM 2232a, a fixed-point cell, designated In 22-2, was constructed from ingots that were randomly selected from the SRM sample lot described in Sec. 2.1. Certification involved the evaluation of both the freezing and melting curves of In 22-2, as well as comparisons with the laboratory indium freezing-point reference cell, designated In 96-2. Both cells are pictured in Fig. 1. Sections 2.2.1 and 2.2.2 describe the cell and the certification process in greater detail.

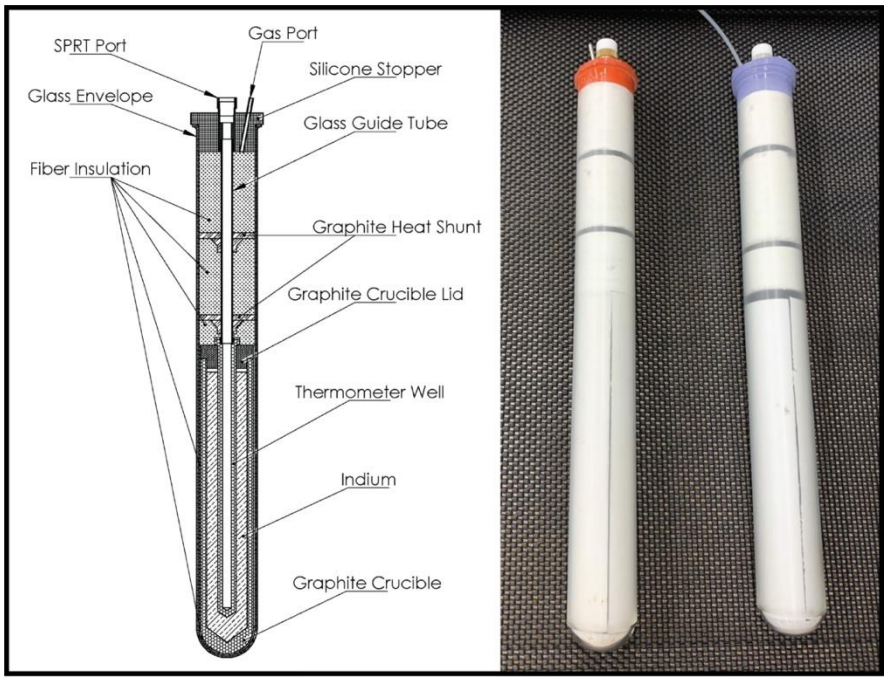

Figure 1. Indium fixed-point cells. On the left is a schematic of a freezing-point cell with relevant cell components labeled. The photograph on the right shows the SRM 2232a fixed-point cell, In 22-2, (purple stopper, right) and the laboratory indium freezing-point reference cell, In 96-1, (red stopper, left). Note that the reference cell used for the measurements reported in this work, In 96-2, remains in use and was not available to be photographed. The cell shown, In 96-1, is an exact replica of In 96-2.

2.2.1. Indium Fixed-Point Cell

A thermometric fixed-point cell (In 22-2) was fabricated following the procedures outlined in Furukawa et al. [4], with a few minor differences. First, in this work, the indium pieces were quite small and, thus, could be added directly to the crucible without use of a graphite “funnel”. Additionally, rather than use an induction furnace to melt the metal, a simple vertical tube furnace, with a setpoint between 160 °C and 170 °C, was used to melt the indium pieces inside the crucible. Finally, all steps were performed under high-purity argon gas, at pressures below 100 kPa.

The completed cell contained (1033 ± 1) g of the high-purity metal randomly selected from the supplied lot. This quantity of material results in an immersion depth of (17.1 ± 0.1) cm, which is the distance from the sensor midpoint of the SPRT to the top of the liquid metal surface. A correction was applied to account for the difference between the immersion depth of In 22-2 and that of the laboratory reference cell (18.0 cm).

During assembly of the cell, any handling of high-purity material is apt to introduce contamination, although every possible effort was made to maintain the purity of the indium and the other fixed-point cell components that contacted the indium. All glassware used during assembly was thoroughly cleaned, followed by at least a 4 h soak in 10% nitric acid and rinsing with copious quantities of distilled water. All handling of indium and graphite components was performed in a laminar flow hood using clean, disposable nitrile gloves. Components were

stored in clean, sealed, polyethylene bags between assembly steps. The melting of indium into the crucible was done under high-purity (nominally 99.999%) argon gas to avoid contamination and oxidation of the fixed-point cell materials.

Since only a limited number of indium pieces could be fit into the crucible at once, multiple fillings were required to add a sufficient amount of indium to the crucible. Indium ingots were placed directly into the graphite crucible to within a few centimeters of the top, melted under an argon atmosphere, and then cooled. This procedure was repeated until enough indium had been added to the crucible. The graphite re-entrant well was inserted into the graphite crucible during the final melt, then the filled graphite crucible was used to assemble the final fixed-point cell.

2.2.2. Temperature Certification Procedure

The first step in the temperature certification process was to obtain several freezing and melting curves using a 25.5 Ω SPRT. These curves were used to assess the sharpness of the phase transition. The second step was to directly compare the cell to the laboratory standard (In 96-2) by simultaneously freezing both the SRM cell and the reference cell. A commercially available 30 Hz AC resistance-ratio bridge (ASL F900) with a thermostatically controlled Tinsley 5685A 100 Ω reference resistor was used to measure the SPRT. These direct comparison measurements provide traceability of the transition temperature to the kelvin, as defined using the ITS-90. Additional details regarding the measurement system can be found in Strouse [5].

Freezing curves were collected following the fixed-point realization procedures outlined in Mangum and Furukawa [6]. Briefly, after melting the cell overnight, the furnace was set to a temperature between 0.3 °C and 0.6 °C below the indium freezing point to initiate the formation of a solid-liquid interface at the crucible wall; nucleation of a solid-liquid interface along the thermometer well was induced via the insertion of room temperature quartz rods into the well. Upon formation of the exterior and interior solid-liquid interfaces, an SPRT was inserted into the cell and thermometer readings were recorded continuously until the freezing was complete, a process which took ten to twenty hours depending on the furnace setpoint. A freeze plateau is considered complete when the temperature in the fixed-point cell falls 10 mK below the maximum temperature on the freezing curve.

After the indium cell was slowly and completely frozen in the above manner, the furnace temperature was set above the freezing-point temperature to slowly melt the metal; the melt plateau was recorded using the same SPRT as was used for the freezing curves. The exact furnace setpoint was varied from curve to curve to achieve melt plateaus lasting from a few hours to nearly two days. Since the shape of the melting curves showed little dependence on melting rate, they can be taken to reflect intrinsic properties of the metal rather than non-equilibrium effects in the furnace-cell setup.

Direct comparison of the fixed-point cell with the laboratory standard fixed-point cell, In 96-2, provides traceability to the ITS-90. To compare the two cells, freeze plateaus were started simultaneously in each cell, which were housed in separate but nearly identical furnaces. Three sets of alternate measurements on their respective freezing-curve plateaus were taken using an

SPRT. This ensures that the comparison measurements on the two cells were made at approximately the same liquid-solid ratio of the metal samples. This procedure was repeated four times.

In this work, the fraction of metal frozen during a set of three measurements of the freezing-point temperature of each cell did not exceed 50%. The SPRT was measured with excitation currents of 1 mA and 1.414 mA to permit extrapolation to zero-power dissipation (0 mA). Corrections were made for differences in pressure and hydrostatic head effects in each cell.

2.3. Determination of Enthalpy of Fusion

2.3.1. Instrument Calibration

A Q2000 DSC from TA Instruments was utilized for the determination of the enthalpy of fusion for SRM 2232a. Prior to measurements of the SRM lot material, careful calibration of the instrument was required to ensure the accuracy of measured temperature and enthalpy. First, a Tzero™ calibration was performed to adjust the instrument's baseline and correct for cell asymmetries. Next, temperature and enthalpy were calibrated via measurements of pure materials with well-known transition temperatures and enthalpies. In this work, two certified reference materials obtained from PTB were used for calibration measurements: indium (SN KM-31402, t_m = 156.598 ± 0.004 °C, ΔH_{fus} = 28.64 ± 0.06 J·g^{-1}) [7] and tin (SN KM-31403, t_m = 231.928 ± 0.004 °C, ΔH_{fus} = 60.24 ± 0.16 J·g^{-1}) [8]. Certified values include expanded (k = 2) uncertainties. Both of these reference materials were certified via comparison with a fixed-point standard and measurements using a modified Tian-Calvet calorimeter for temperature and enthalpy, respectively [7, 8].

The determination of both the temperature and enthalpy calibration parameters are represented schematically in Fig. 2, where the gray line represents a theoretical melting curve. The temperature used is the extrapolated onset temperature (t_e), which is determined from the intersection of the inflectional tangent line (red dashed line) and the interpolated baseline (blue dashed line) (Fig. 2). This is used instead of the peak maximum/minimum temperature because it is less dependent on the heating rate and sample parameters such as sample thermal conductivity, sample mass, and sample thickness [9-11].

With DSC, energy is determined by integrating the heat flow signal over time and multiplying by a proportionality constant (K_q). K_q is calculated by dividing the reference transition enthalpy (ΔH_{ref}) by the experimental transition enthalpy (ΔH_{exp}) (see Fig. 2). The certified values obtained from the respective calibration certificates were used for the former, while the latter was obtained by integrating the experimentally determined melting curves (shaded gray in Fig. 2).

In this work, five samples for each of the two calibration materials were encapsulated in hermetically sealed aluminum pans. All mass measurements employed a microbalance and a double-substitution (ABBA) weighing scheme [12]; additional details regarding sample preparation can be found in Fortin et al. [13]. For the certified indium samples, masses ranged from 6.738 mg to 13.386 mg, including two samples with masses of ~ 8.4 mg. The certified tin

sample masses ranged from 7.182 mg to 13.866 mg and also included two samples with masses of ~ 8.4 mg.

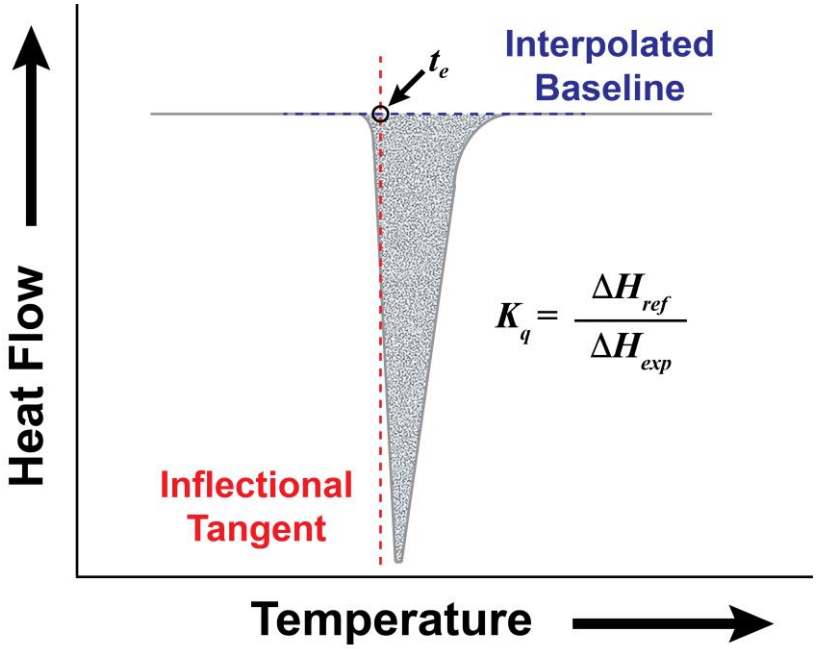

Figure 2. Determination of temperature and enthalpy calibration parameters. The gray line represents a theoretical melting curve. The extrapolated onset temperature (t_e) is used for the temperature calibration. The integrated peak area (shaded gray) is used to determine the enthalpy calibration coefficient (K_q).

For all calibration measurements the procedure was as follows. A sample pan was loaded into the measurement cell, along with an empty reference pan (also hermetically sealed and aluminum). The cell was then equilibrated at a temperature significantly below the melting point (i.e., 100 °C and 170 °C for indium and tin, respectively) before heating at a given heating rate (β) to a temperature sufficiently above the melting point to reestablish a stable baseline (i.e., 180 °C and 270 °C for indium and tin, respectively). Since the primary measurements associated with DSC are very sensitive to the specific experimental conditions employed (e.g., the sample size and form, sample placement within the pan, pan type, pan placement within the cell, heating rate employed, purge gas used, etc.), temperature and enthalpy calibrations should be carried out using the same conditions as will be used for sample measurements [9-11]. Therefore, after an initial "premelt" run at β = 20 °C·min^{-1}, each sample pan was measured twice at four heating rates in the order: 1 °C·min^{-1}, 10 °C·min^{-1}, 3 °C·min^{-1}, and 5 °C·min^{-1}. Sample pan selection was randomized but no back-to-back runs of a given pan were permitted; this was done to ensure that a sample pan was always placed anew at the start of each run thus capturing any variability in the results attributable to pan placement. All indium calibration measurements at a given heating rate were completed before moving on to the next heating rate, and all indium measurements were completed before repeating the procedure with the certified tin samples. Additionally, at each heating rate, multiple baseline checks were

performed before, during, and after calibration measurements to check for evidence of deterioration in the instrument's performance; no such evidence was observed. Finally, for all measurements, dry nitrogen was used as a purge gas at a flow rate of 50 mL·min^{-1}.

Upon completion of the calibration measurements, the individual melting curves were analyzed to determine both t_e and K_q. Although several literature sources recommend extrapolating to zero heating rate to determine a temperature correction [14, 15], the ASTM standard test method for DSC temperature calibration (E967) [16] calls for calibration at the heating rate of interest. We have used the β-specific approach in this work. Therefore, an overall average t_e, encompassing all sample sizes and replicate measurements, was calculated for each heating rate for both indium and tin; the results are reported in Table 2. Prior to the start of SRM 2232a indium measurements at a given heating rate, the corresponding calibration parameters were entered into the instrument's software. It should be noted that with a two-point calibration, the instrument's software assumes a linear relationship to interpolate between the entered temperatures. For the enthalpy calibration, we followed literature recommendations [14, 15] and determined K_q as a function of temperature, as well as heating rate. However, since all subsequent experiments would focus on measurements of indium and no significant mass dependence was observed in the calibration data, we ultimately used the indium results alone to calculate an average K_q including all sample masses and replicate measurements. The resulting β-specific values, which are reported in Table 2, were used for all subsequent SRM 2232a indium measurements.

Table 2. Instrument Calibration Parameters Used During SRM Indium Measurements.

β^a (°C·min^{-1})	Indium $t_e{}^b$ (°C)	Tin $t_e{}^b$ (°C)	$K_q{}^c$
1	156.393	231.305	1.05517
3	156.389	231.298	1.05331
5	156.389	231.292	1.05531
10	156.354	231.272	1.05941

[a]Nominal heating rate. [b]Averaged extrapolated onset temperature. [c]Averaged enthalpy calibration coefficient.

2.3.2. Enthalpy of Fusion Measurements

For the SRM 2232a measurements, a total of 15 samples were prepared from 7 randomly selected ingots of the SRM indium lot labeled "A" through "G". For each ingot, a dedicated new and freshly cleaned razor was used to retrieve slices of sample of the desired mass for encapsulation in hermetically sealed aluminum pans. Additional information regarding sample preparation can be found in Sec. 2.3.1 and the references cited therein. Overall, SRM indium sample masses ranged from 7.296 mg to 13.663 mg, with several samples of ~ 8 mg. Individual sample masses are reported in Table 3.

In addition to the SRM indium samples listed in Table 3, three fresh samples of the indium calibration material were prepared to check the calibrated instrument's performance against PTB's certified temperature and enthalpy values. The masses of these indium check samples were 6.962 mg, 8.429 mg, and 9.357 mg.

Table 3. Indium Samples Used for SRM 2232a Enthalpy Measurements.

Sample	Mass (mg)
A1	8.118
A2	8.078
A3	8.011
A4	8.148
A5	8.163
B1	8.146
B2	8.233
B3	8.224
C	13.663
D	7.574
D2	7.296
E	10.647
F	9.551
G	13.258
G2	13.185

The SRM 2232a enthalpy of fusion measurements followed the previously described procedure employed for the calibration measurements (see Sec. 2.3.1). The indium check samples were incorporated with the SRM samples during these measurements. As was the case with the calibration samples, all of the SRM and check samples underwent an initial "premelt" run at β = 20 °C·min^{-1}. However, for these measurements, each sample was measured a total of three times at each of the four heating rates (1 °C·min^{-1}, 10 °C·min^{-1}, 3 °C·min^{-1}, and 5 °C·min^{-1}). Prior to measurements at a given heating rate, the corresponding β-specific calibration parameters from Table 2 were entered into the instrument's software. Once again, regular baseline checks were performed during each measurement series. In addition, a single indium verification measurement was performed after each baseline check using one of the ~ 8 mg certified indium samples previously used for the calibration measurements. These baseline and indium

verification measurements were used to verify that the instrument was operating within specifications for the duration of the SRM 2232a enthalpy measurements.

3. Experimental Results

3.1. Melting Temperature Results

Figure 3 shows the freezing curves collected for the SRM indium fixed-point cell, In 22-2. The duration of a freeze varied from 9 h to 21 h and was dictated by the furnace setpoint (see Sec. 2.2.2). To normalize the freezing curves, time was converted to "fraction frozen" (*F*) by assuming that *F* increases linearly with time from the onset of data collection (*F* = 0) to the point where the cell has frozen (*F* = 1), where the latter is defined as the time when the temperature measured by the SPRT has fallen 10 mK below the temperature of the plateau. For comparison purposes, the freezing curves were also normalized so that the SPRT resistance obtained during the beginning of the freezing-point realization (defined as the average reading between *F* = 0.02 and *F* = 0.05) was equivalent to 0 mK.

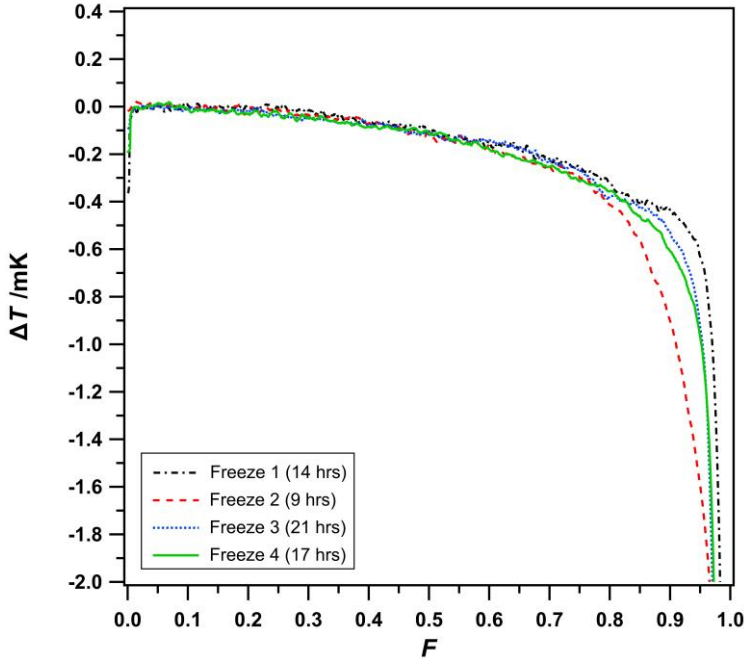

Figure 3. Freezing curves for the SRM fixed-point cell In 22-2, plotted as change in temperature (Δ*T*) as a function of fraction frozen (*F*). Shown are freezing curves measured on different days; the duration of the freeze is dictated by the furnace setpoint. The curves have been smoothed slightly to improve curve differentiation.

Analysis of the freezing curve plateaus gives insight into the total impurity level in the indium metal. Best practices for estimating the effect of impurities on the freezing behavior of fixed-point cells are described in the Guide to the Realization of the ITS-90 [17]. Analysis of impurities in the indium metal allows us to set a bound on the offset of the fixed-point cell freezing temperature from that of an ideal sample of pure indium, which defines the ITS-90 indium fixed point. As the cell freezes, impurities tend to segregate into the liquid or solid phases depending on the identity of the impurity. This segregation changes the effective

concentration of the impurities in the remaining liquid, which in turn leads to a changing freezing temperature; this is the origin of the slight slope to the freezing curves shown in Fig. 3.

The slope of the freezing curves, coupled with Raoult's Law of dilute solutions, can also be used to place a lower bound on impurities in the cell [17]. This is an important check, since contamination during cell fabrication could introduce impurities beyond those measured in the assay of the indium samples. The average temperature depression when 50% of the metal was frozen was 0.10 mK. Using Raoult's Law, this sets a lower limit on the impurity concentration of 0.2 $\mu g \cdot g^{-1}$.

Following the guidance of the Guide to the Realization of the ITS-90 [17], the total estimated impurity concentration should include all detected impurities and one-half of the detection limit of other common impurities. As discussed in Sec. 2.1, the GDMS purity analysis results for the SRM indium show detected impurities of approximately 0.11 $\mu g \cdot g^{-1}$, while the detection limits for 15 additional common impurities total approximately 0.21 $\mu g \cdot g^{-1}$ (see Fig. A.1.1 of Appendix A.1). When combined, these results indicate an estimated impurity concentration of 0.21 $\mu g \cdot g^{-1}$, consistent with the above analysis based on freezing curve slope. While these methods allow one to assign an uncertainty, *a priori*, for the effect of impurities on the freezing temperature of the fixed-point cell, it is often more practical to link the cell to the ITS-90 through direct comparison to another fixed-point cell, as is discussed below.

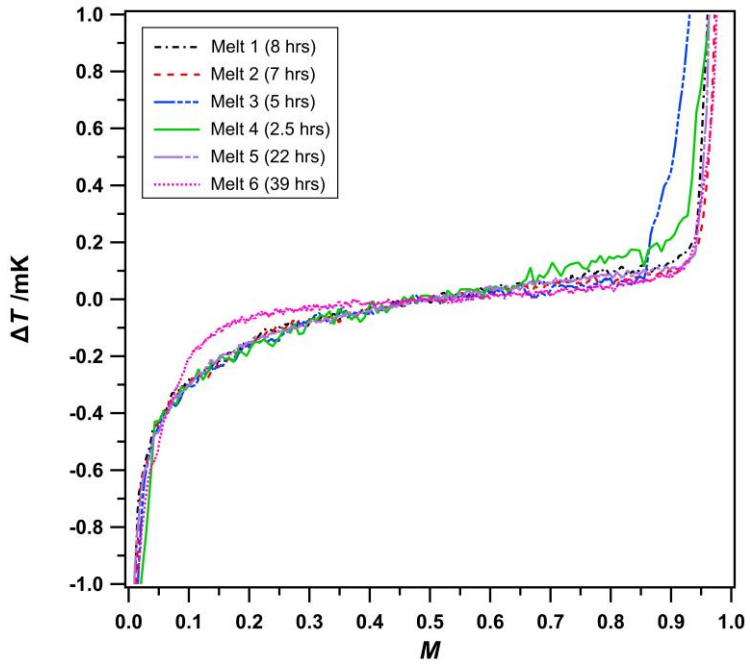

Figure 4. Melting curves for the SRM fixed-point cell In 22-2, plotted as change in temperature (ΔT) as a function of fraction melted (M). Shown are melting curves measured on different days; the duration of the melt is dictated by the furnace setpoint. The curves have been smoothed slightly to improve curve differentiation.

Figure 4 shows the melting curves for In 22-2, with the furnace set to various temperatures above the melting point. The melts lasted between 2.5 h and 39 h. For comparison purposes, the melting curves were normalized so that the SPRT resistance when 50% of the indium had melted (M = 0.5) passes through the 0 mK point on the graph; the M = 0 and M = 1 points were defined as the points 10 mK below and above the temperature at the M = 0.5 point, respectively. From the curves in Fig. 4, the average temperature range of the melting curves, measured from M = 0.2 to M = 0.8, was 0.22 mK. The average difference in the liquidus-point temperatures determined from the freezing and melting curves for the SRM cell was 0.02 mK, which is an indication of a good cell.

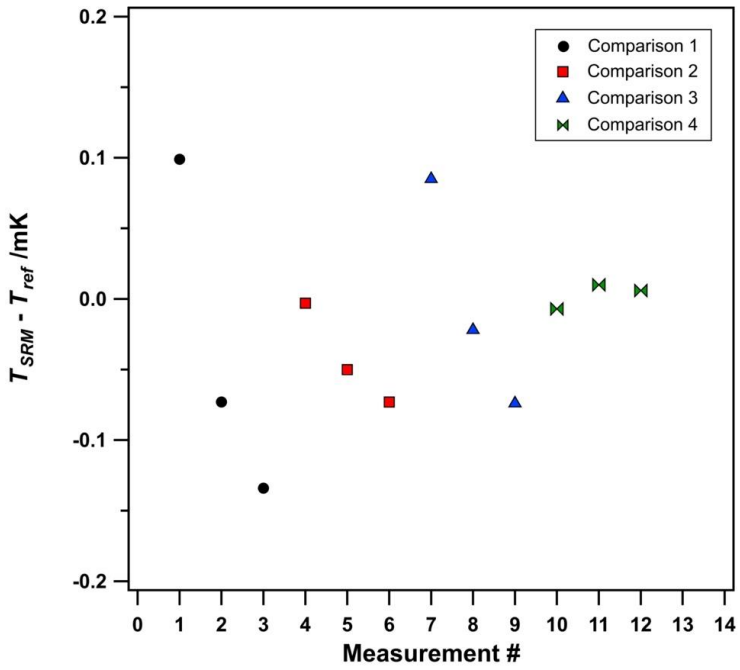

Figure 5. Direct comparison results for the SRM cell, In 22-2, with the NIST laboratory reference standard, In 96-2. Results are plotted as In 22-2 temperature (T_{SRM}) minus In 96-2 temperature (T_{ref}) as a function of measurement number. Different symbols indicate distinct sets of comparison measurements, performed in triplicate.

The second part of the certification was a direct comparison of the SRM fixed-point cell under test with the laboratory standard fixed-point cell (In 96-2). The results for four separate comparisons, each consisting of three sets of measurements of the cells' respective freezing-curve plateaus, are shown in Fig. 5. An SPRT was measured first in the SRM fixed-point cell, then moved to the laboratory standard cell, allowed to equilibrate, and measured. The SPRT was then returned to the SRM fixed-point cell, and the procedure repeated twice more. After completion of three measurements, both cells were completely melted overnight before repeating the comparison during new freeze plateaus. Comparisons one through three show a decreasing trend between measurements indicating that the SRM fixed-point cell was proceeding along its freeze plateau more quickly than the laboratory standard cell, most likely

due to slight differences in their respective furnace temperature offsets. On average, In 22-2 was 0.02 mK colder than the laboratory standard.

3.2. Enthalpy of Fusion Results

Upon completion of the SRM 2232a indium measurements, each of the resulting melting curves were analyzed to determine the enthalpy of fusion (ΔH_{meas}). An example of this analysis is shown in Fig. 6 for sample A1 measured at β = 3 °C·min^{-1}. First, a linear baseline was drawn between two points indicating the start and stop of the melting peak (at 155 °C and 165 °C, respectively, for this example). The peak was then integrated between these two points to determine the area (mW·s), which was then divided by the sample mass to determine ΔH_{meas} (J·g^{-1}). The results for each individual replicate measurement are reported in Table A.2.1 of Appendix A.2. To aid in comparisons, the ΔH_{meas} results reported in Table A.2.1 are also shown in Fig. 7, plotted as a function of nominal heating rate. Here, the source ingots are distinguished by seven distinct markers and the ingot subsamples are differentiated by color. The greatest overall variability is observed at β = 1 °C·min^{-1}, but this primarily attributed to a couple of outlying measurements; if these points are ignored, the observed variabilities are similar at all four heating rates.

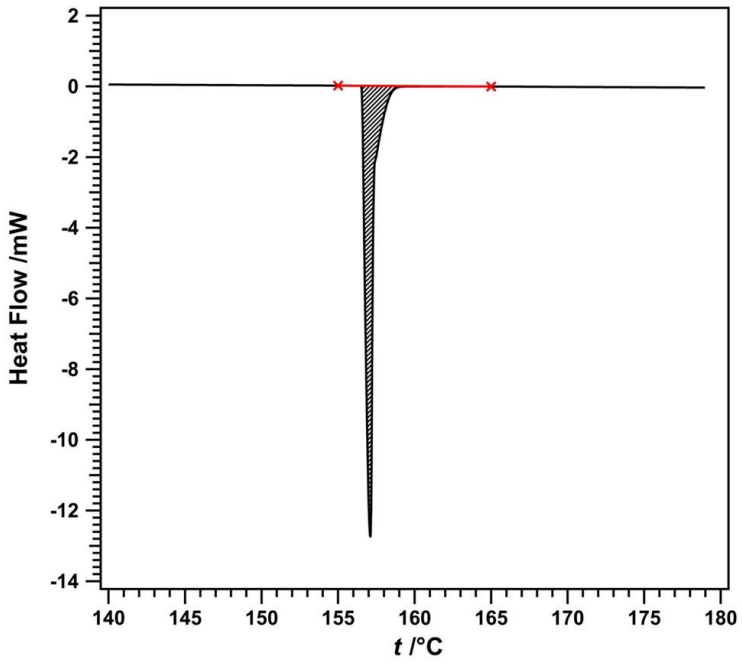

Figure 6. Determination of enthalpy of fusion. Shown in black is the heat flow curve plotted as a function of temperature for a single replicate measurement of sample A1 at 3 °C·min^{-1}. A linear baseline (red) was drawn between points on either side of the peak (red x's at 155 °C and 165 °C in this example). The peak was then integrated to get the area (hatch marks) in mW·s, which was divided by the sample mass to obtain the enthalpy of fusion.

The goal was to use the measurement results shown in Fig. 7 to derive a single enthalpy of fusion and its associated uncertainty for each of the measured heating rates (ΔH_β and $u(\Delta H_\beta)$, respectively). However, as was previously discussed, DSC measurements are highly sensitive to experimental parameters such as heating rate, and each individual instrument will presumably exhibit its own particular dependency. As such, β-dependent information is only of limited use; for a certified reference material the enthalpy of fusion at thermal equilibrium is the value of interest for consumers. Therefore, ultimately, we want to determine the enthalpy of fusion at β = 0 °C·min^{-1}.

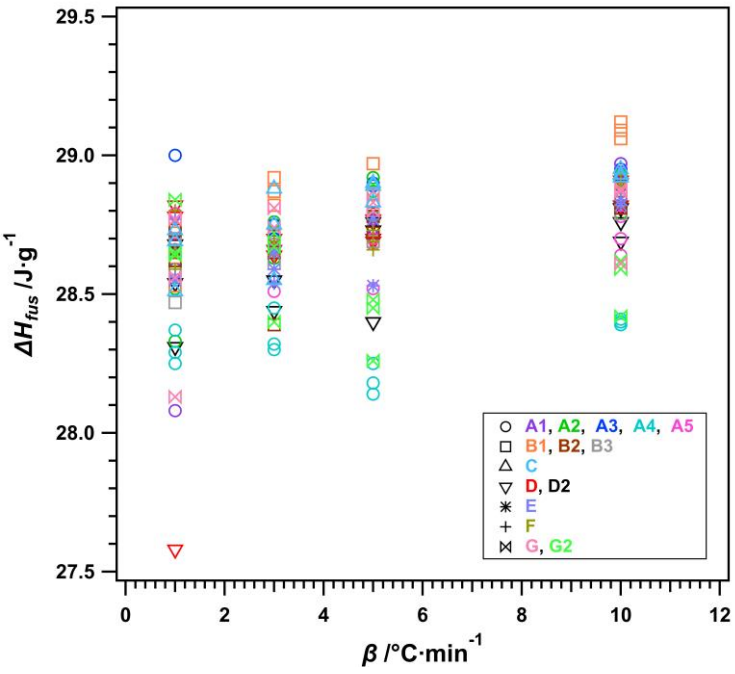

Figure 7. Replicate enthalpy of fusion measurement results for fifteen SRM 2232a samples plotted as a function of nominal heating rate. Samples sourced from seven different ingots are plotted as distinct markers and ingot subsamples are differentiated by color, as indicated by the included legend.

In this work, we have used a hierarchical Bayesian model [18] to determine ΔH_β and $u(\Delta H_\beta)$ as a function of heating rate, including at β = 0 °C·min^{-1}. With this type of model, we can easily account for correlations in the data induced by using the same subsamples across different β values. Additionally, this approach is able to handle the fact that the actual β values differ slightly from the nominal. Specifically, for each measured enthalpy of fusion value, we assumed

$$\Delta H_{meas,ijk} = \alpha_0 + \alpha_1 \cdot \beta_{ijk} + A_i + B_{ij} + \epsilon_{ijk} + S_l \, . \quad (1)$$

Here, α_0 is the intercept, which corresponds to the value at β = 0 °C·min^{-1} (i.e., ΔH_{fus}), and α_1 is the slope. The "ijk" subscript indicates the k^{th} measurement for the j^{th} subsample within the i^{th} sample. In this work, i = 1,...,7 and j = 1,...,$n_{j(i)}$, with the number of subsamples, $n_{j(i)}$, within each sample varying from 1 to 5. A_i accounts for sample effects and was assumed to have a normal distribution with an expected value of zero and a variance of σ_A^2 (i.e., A_i ~ Normal(0, σ_A)). Similarly, B_{ij} accounts for subsample effects and B_{ij} ~ Normal(0, σ_B). Next, ϵ_{ijk} represents the measurement error due to random effects. To allow for possible outlying points, such as subsample 1 of sample D (e.g., sample D in Table 3) at β = 1 °C·min^{-1} (see Fig. 7), we assumed ϵ_{ijk} has a Student's t-distribution with four degrees of freedom, an expected value of 0, and a scale selected such that its variance is equal to σ_ϵ^2. Finally, S_l represents the β-specific subsample effect with S_l ~ Normal(0, $\sigma_{S,l}$). Here, l indicates the associated nominal heating rate (i.e., $l \in$ 1,...,4 corresponding to β = 1, 3, 5, or 10 °C·min^{-1}). To determine $\sigma_{S,l}$ we calculated the uncertainty due to systematic effects, $u(\Delta H_{meas})$, and used the mean at each nominal β. The determination of $u(\Delta H_{meas})$ is discussed in detail in Sec. 4.2.

We used a Bayesian analysis to fit the model in Eq. (1). In a Bayesian analysis, we are interested in the posterior distribution of the parameters of interest, $\boldsymbol{\theta} = (\alpha_0, \alpha_1, \sigma_A, \sigma_B, \sigma_\epsilon, \mathbf{A}, \mathbf{B}, \mathbf{S})$, which is proportional to the prior distribution, $p(\boldsymbol{\theta})$, multiplied by the likelihood of the observed data, $p(\mathbf{x}|\boldsymbol{\theta})$. Mathematically, this is written as

$$p(\boldsymbol{\theta}|\mathbf{x}) \propto p(\boldsymbol{\theta})p(\mathbf{x}|\boldsymbol{\theta}). \tag{2}$$

The likelihood, $p(\mathbf{x}|\boldsymbol{\theta})$, is the probability density for the observed data at $\mathbf{x} = (\mathbf{H}, \boldsymbol{\beta}, \boldsymbol{\sigma_S})$ given a set of parameters $\boldsymbol{\theta}$. It is determined by the model and distributions described below. Here, $\mathbf{H}$ and $\boldsymbol{\beta}$ represent the $\Delta H_{meas,ijk}$ and β_{ijk} for all i, j, and k values and $\boldsymbol{\sigma_S}$ represents $\sigma_{S,l}$ for $l \in$ 1,...,4.

The prior distribution, $p(\boldsymbol{\theta}) = p(\alpha_0, \alpha_1, \sigma_A, \sigma_B, \sigma_\epsilon, \mathbf{A}, \mathbf{B}, \mathbf{S})$, encompasses our prior knowledge or beliefs about the unknown parameters of interest and is composed of the individual prior distributions for each parameter. Prior distributions specify what we know about these parameters before any data has been collected and can be defined to incorporate realistic bounds, scientific judgment, or can cover a wide range of values to specify no prior knowledge.

For this analysis, we assumed *a priori* that α_0 ~ Normal(28, 10), which puts 95% of the prior probability between 8.4 and 47.6. For the slope, we assume α_1 is restricted to positive numbers because a negative slope is scientifically implausible and that α_1 follows a truncated Normal(0, 10) distribution, which puts 95% of the prior probability between 0.31 and 22.42. These can be thought of as relatively flat prior distributions, spreading the prior probability between a wide range of numbers.

For the uncertainty parameters, σ_A, σ_B, and σ_ϵ, we assumed half Student's t-distributions, bounded to be $\geq$ 0 since uncertainties must be positive, centered at zero, with a scale equal to 0.21, and with four degrees of freedom, which puts roughly 95% of the prior probability

between 0.01 and 0.73. This distribution has a long tail, putting most of the prior weight on smaller values of these parameters but allowing for values that are larger if there is strong evidence in the data for larger uncertainties. We performed a sensitivity analysis, varying the size of the scales for these half Student's *t*-distributions, and found that the results reported below were not very sensitive to changes in these prior assumptions.

Once the prior distributions and the likelihood were defined, we then used Hamiltonian Monte Carlo, implemented via Stan [19] using the R [20] package "rstan" [21], to sample from the posterior distribution. From these samples we then estimated the mean of the posterior distribution, as well as 95% intervals that encompassed our uncertainties for these parameter values.

Specifically, from the Bayesian analysis we sampled from the posterior distributions of the model parameters, and we used posterior samples of the intercept and slope to calculate estimates and uncertainties of the enthalpy of fusion at different β values. In Table 4 we report estimated enthalpies of fusion for each β of interest (i.e., posterior means, ΔH_β), associated uncertainties (i.e., posterior standard deviations, $u(\Delta H_\beta)$), and the lower and upper bounds of 95% credible intervals (*LB* and *UB*, respectively). These bounds were calculated as the 2.5 and 97.5 percentiles of the posterior samples. Also included in Table 4 are the expanded uncertainties ($U(\Delta H_\beta)$), calculated from the lower and upper bounds using (*UB* – *LB*)/2, and the expansion factor *k*, calculated as $U(\Delta H_\beta)/u(\Delta H_\beta)$. It should be noted that predictive checks were performed to validate the modeling approach used in this work, the results of which indicate that the proposed model is indeed reasonable (see Appendix A.3).

Table 4. Enthalpy of Fusion as a Function of Heating Rate Calculated Using the Hierarchical Bayesian Model.

β[a] (°C·min^{-1})	ΔH_β[b] (J·g^{-1})	$u(\Delta H_\beta)$[c] (J·g^{-1})	*LB*[d] (J·g^{-1})	*UB*[e] (J·g^{-1})	$U(\Delta H_\beta)$[f] (J·g^{-1})	*k*[g]
0	28.58	0.09	28.40	28.75	0.17	1.93
1	28.61	0.08	28.45	28.76	0.16	1.94
3	28.67	0.07	28.53	28.80	0.14	1.97
5	28.72	0.08	28.57	28.87	0.15	1.96
10	28.87	0.14	28.63	29.15	0.26	1.91

[a]Nominal heating rate. [b]Heating-rate specific enthalpy of fusion (posterior means) determined using the hierarchical Bayesian model (Eq. (1)). [c]Uncertainty for heating-rate specific enthalpy of fusion (posterior standard deviations) [d]Lower bounds of 95% credible intervals. [e]Upper bounds of 95% credible intervals. [f]Expanded uncertainty calculated from uncertainty bounds as (*UB* – *LB*)/2. [g]Expansion factor calculated as $k = U(\Delta H_\beta)/u(\Delta H_\beta)$.

As was previously mentioned, the value that is of primary interest for a certified reference material is the enthalpy of fusion at thermal equilibrium (i.e., at β = 0 °C·min^{-1}). Table 4 shows

that for SRM 2232a that value is 28.58 J·g^{-1}; we refer to this as ΔH_{fus} and it is the certified value that appears in Table 1 and is reported in the certificate. Explicitly reporting ΔH_{fus} at β = 0 °C·min^{-1} is an important improvement over the earlier version of this SRM. From the available documentation for SRM 2232 [1], it is unclear at what heating rate, or rates, the enthalpy of fusion measurements were performed or if the reported certified value of 28.51 J·g^{-1} was at β = 0 °C·min^{-1} or some other heating rate. Finally, the ΔH_{β} and $U(\Delta H_{\beta})$ values reported in Table 4 at the other four heating rates are also included in the certificate for SRM 2232a for reference.

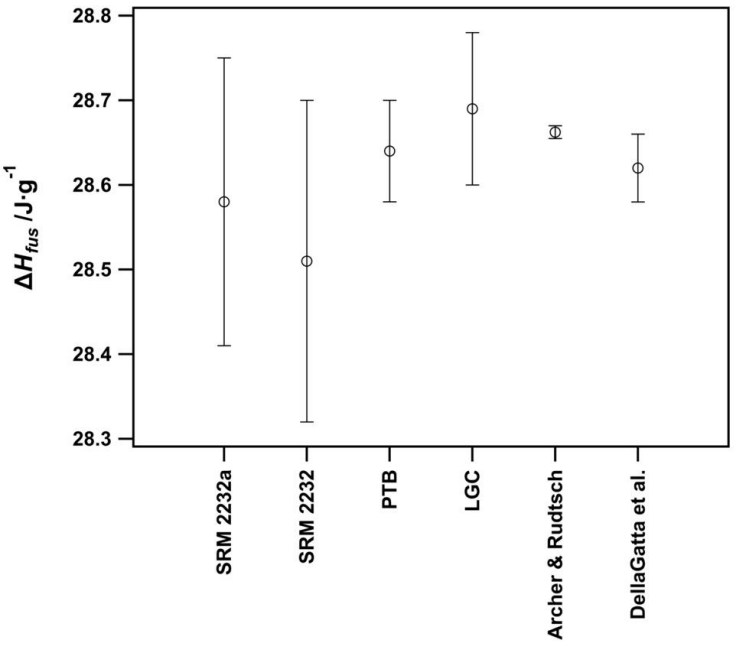

Figure 8. Comparison of enthalpy of fusion values. The certified value for SRM 2232a is compared to that of the previous SRM (SRM 2232 [1]), and two currently available certified reference materials from PTB [7] and LGC [22]. Two additional literature values from the work of Archer and Rudtsch [23] and Della Gatta et al. [14] are also shown. Error bars represent reported expanded ($k \approx 2$) uncertainties.

In Fig. 8 we have compared the certified enthalpy of fusion for SRM 2232a with that of the previous SRM [1], as well as two other certified reference materials currently available from PTB [7] and LGC [22]. Also shown in Fig. 8 are two values taken from the literature. The first was reported by Archer and Rudtsch [23], and is based on adiabatic calorimetry measurements. The second, reported by Della Gatta et al. [14], is the value recommended by the International Union of Pure and Applied Chemistry (IUPAC) for use in DSC calibration and is the result of a critical evaluation of all available literature values for the enthalpy of fusion for indium [24]. As is shown in Fig. 8, the certified enthalpy of fusion values for both SRM 2232a and its predecessor, SRM 2232, have larger associated uncertainties than the other values; this is not surprising given that both SRM values were determined via DSC measurements, which is inherently more uncertain than either the Calvet calorimetry measurements of PTB and LGC [7,

22] or the adiabatic calorimetry measurements of Archer & Rudtsch [23]. Additionally, Fig. 8 demonstrates that, although the certified enthalpy of fusion for SRM 2232a is slightly lower than all but SRM 2232, it agrees with all other values well within reported uncertainties.

4. Uncertainty Analysis

4.1. Melting Temperature Uncertainty

Since traceability to the ITS-90 is provided through the direct comparison measurements, the uncertainty of those measurements directly affects the total uncertainty of the SRM melting temperature. The uncertainty of the NIST reference cell (In 96-2) is well documented [5]. By virtue of its identical cell design and identical measurement system, the uncertainty budget for In 96-2 includes all the components that one would expect to be present in a measurement of In 22-2, the estimates for which are shown in Table 5 and include both type A (based on data) and type B (based on other sources) evaluations of uncertainties [25]. The only component that we need to evaluate anew is that introduced by the direct comparison measurements themselves. Here, the direct comparison repeatability was derived from the standard deviation of the 12 comparison measurements and is shown as the first item in Table 5. Also shown is the total combined standard uncertainty in the direct comparison measurements, $u(DC)$, which is estimated at 0.069 mK and was calculated as the root sum of squares of the individual uncertainty components.

Table 5. Estimated Uncertainty from Direct Comparison Measurements.

Component	Type	Distribution	$u(z)^a$ (mK)
Direct comparison repeatability	A	Normal	0.064
Bridge repeatability	A	Normal	0.002
Bridge non-linearity	A	Normal	0.021
AC bridge quadrature	B	Rectangular	0.003
Reference resistor stability	B	Rectangular	0.003
Hydrostatic head correction	B	Rectangular	0.005
SPRT self-heating	B	Rectangular	0.006
Heat flux	B	Normal	0.002
Gas pressure	B	Rectangular	0.011
$u(DC)^b$			0.069

[a]Standard (k = 1) uncertainty estimate for the corresponding component. [b]Combined standard uncertainty from direct comparison measurements. Calculated as the root sum of squares of the individual uncertainty components.

Table 6 shows the uncertainty budget for the SRM fixed-point cell. In addition to the uncertainty from the direct comparison measurements, the combined standard uncertainty in the melting point temperature of the SRM includes contributions from the uncertainty of the NIST reference cell, In 96-2, as well as two type B uncertainty evaluations corresponding to the average difference between the In 22-2 freezing and melting curves and to the average temperature range of the In 22-2 melting curves. The root sum of squares of the individual

components listed in Table 6 yields a combined standard uncertainty in the SRM melting temperature, $u(t_m)$, of 0.16 mK. The expanded (k = 2) uncertainty for the certified melting temperature of SRM 2232a, $U(t_m)$, is thus 0.32 mK, which is the value that appears in Table 1 and is reported in the certificate.

Table 6. Estimated Total Uncertainty in Melting Temperature.

Component	Type	Distribution	$u(z)^a$ (mK)
Direct comparison measurements			0.064
NIST reference cell			0.089
Difference between melt and freeze curves	B	Normal	0.023
Melt curve width	B	Normal	0.11
$u(t_m)^b$			0.16
$U(t_m)^c$			0.32

[a]Standard (k = 1) uncertainty estimate for the corresponding component. [b]Combined standard uncertainty in the melting temperature. Calculated as the root sum of squares of the individual components. [c]Expanded (k = 2) uncertainty in the melting temperature.

4.2. Enthalpy of Fusion Uncertainty Due to Systematic Effects

For enthalpy of fusion, measurement uncertainty can be attributed to both systematic and random effects. In this work, the hierarchical Bayesian model described in Sec. 3.2 accounts for both of these components. However, the uncertainty due to systematic effects must be supplied to the Bayesian model. Our approach to estimating this uncertainty is described here.

A single measurement of the enthalpy of fusion, ΔH_{meas}, for a given sample at a single heating rate can be expressed as

$$\Delta H_{meas} = \frac{x}{m}, \tag{3}$$

where x is the integrated peak area (mW·s) and m is the sample mass (mg). The combined standard uncertainty attributed to systematic effects, $u(\Delta H_{meas})$, can then be expressed as

$$u(\Delta H_{meas}) = \sqrt{\left(\frac{1}{m}\right)^2 u^2(x) + \left(\frac{-x}{m^2}\right)^2 u^2(m)}, \tag{4}$$

where the uncertainty in the integrated peak area, $u(x)$, can be estimated from simulation, and the uncertainty in mass, $u(m)$, is estimated at 0.003 mg. The individual uncertainty components are discussed in more detail in Secs. 4.2.1 and 4.2.2. In this work, $u(\Delta H_{meas})$ was determined for each replicate measurement for all 15 samples at each nominal β; the β-specific mean uncertainties were then determined and used as model inputs (i.e., $\boldsymbol{\sigma_S}$). Specifically, the $\boldsymbol{\sigma_S}$ values used in this work were 0.091, 0.074, 0.106, and 0.187 J·g^{-1} at 1, 3, 5, and 10 °C·min^{-1}, respectively.

4.2.1. Uncertainty in Integrated Peak Area ($u(x)$)

We employed a simulation study to estimate the standard uncertainty in the integrated peak area, $u(x)$. This allowed us to incorporate variability arising from the selection of the baseline endpoints, as well as individual heat flow measurements. We assumed that time was measured without statistically significant error and, therefore, did not incorporate variability from those measurements in our simulations.

To address heat flow measurement variability, we first had to estimate the uncertainty associated with the heat flow signal recorded by the instrument. Recorded heat flow, HF_{record}, can be expressed as

$$HF_{record} = K_q \cdot HF_{raw}\,, \tag{5}$$

where K_q is an (unitless) enthalpy calibration coefficient and HF_{raw} is the raw (i.e., uncalibrated) heat flow signal (mW). The standard uncertainty in the recorded heat flow, $u(HF_{record})$, can then be expressed as

$$u(HF_{record}) = \sqrt{(HF_{raw})^2 u^2(K_q) \; + \; (K_q)^2 u^2(HF_{raw})}\,. \tag{6}$$

As was previously discussed (Sec. 2.3.1), K_q was obtained by measuring materials with known transition enthalpies and calculating the ratio of the reference transition enthalpy, ΔH_{ref} (J·g^{-1}), to the experimentally determined transition enthalpy, ΔH_{cal} (J·g^{-1}):

$$K_q = \frac{\Delta H_{ref}}{\Delta H_{cal}} + C\,. \tag{7}$$

Here, C represents an additional systematic uncertainty contribution associated with the enthalpy calibration. The standard uncertainty in K_q, $u(K_q)$, can then be expressed as

$$u(K_q) = \sqrt{\left[\frac{\partial K_q}{\partial \Delta H_{ref}}\right]^2 u^2(\Delta H_{ref}) + \left[\frac{\partial K_q}{\partial \Delta H_{cal,avg}}\right]^2 u^2(\Delta H_{cal,avg}) + u^2(C)}\,. \quad (8)$$

In Eq. (8), the two partial derivatives are defined as follows:

$$\frac{\partial K_q}{\partial \Delta H_{ref}} = \frac{1}{\Delta H_{cal,avg}} \text{ and} \quad (9)$$

$$\frac{\partial K_q}{\partial \Delta H_{cal,avg}} = -\frac{\Delta H_{ref}}{(\Delta H_{cal,avg})^2}\,. \quad (10)$$

The calibration certificate for the indium certified reference material used in this work reports an expanded (k = 2) uncertainty of 0.06 J·g^{-1} [7], therefore the standard uncertainty associated with the reference enthalpy, $u(\Delta H_{ref})$, is 0.03 J·g^{-1}. The random uncertainty associated with the enthalpy calibration measurements, $u(\Delta H_{cal,avg})$, can be defined as

$$u(\Delta H_{cal,avg}) = \frac{s_{\Delta H_{cal,avg}}}{\sqrt{10}}, \quad (11)$$

where $\Delta H_{cal,avg}$ is the average enthalpy of fusion and $s_{\Delta H_{cal,avg}}$ is the sample standard deviation (J·g^{-1}) of the 10 enthalpy calibration measurements discussed in Sec. 2.3.1. The β-specific values used in the above equations are shown in Table 2 for K_q and in Table 7 for $\Delta H_{cal,avg}$, and $s_{\Delta H_{cal,avg}}$.

The final term in Eq. (8) was estimated by comparing the results of the indium check measurements (Sec. 2.3.2) with PTB's certified enthalpy value. Based on those comparisons, we conservatively estimate that the enthalpy calibration contributes an additional systematic error to the resulting K_q values, the value of which depends on the heating rate. Assuming this error represents the bounds on a uniform distribution, the standard uncertainty from the enthalpy calibration, $u(C)$, is then expressed as

$$u(C) = \frac{(p/100)}{\sqrt{3}}, \tag{12}$$

where p is the percent error; p is estimated to be 0.3% at 1 °C·min^{-1} and 3 °C·min^{-1}, 0.5% at 5 °C·min^{-1}, and 1.1% at 10 °C·min^{-1}.

Table 7. Averaged Measured Enthalpy of Fusion from Ten Indium Calibration Measurements as a Function of Heating Rate.

β^a (°C·min^{-1})	$\Delta H_{cal,avg}{}^b$ (J·g^{-1})	$s_{\Delta H_{cal,avg}}{}^c$ (J·g^{-1})
1	27.144	0.207
3	27.191	0.134
5	27.140	0.181
10	27.035	0.173

[a]Nominal heating rate. [b]Averaged measured enthalpy of fusion. [c]Standard deviation.

Finally, in Eq. (6), the uncertainty in the raw heat flow signal, $u(HF_{raw})$, is estimated by converting the manufacturer's "baseline reproducibility" to a standard uncertainty based on the assumption that the manufacturer's specifications represent bounds for a uniform distribution:

$$u(HF_{raw}) = \frac{0.01}{\sqrt{3}} = 0.0057735 \text{ mW}. \tag{13}$$

Using Eq. (6), $u(HF_{record})$ was calculated as a function of time for each of the measured heat flow curves; these uncertainty values defined boundaries for the subsequent simulations. Specifically, customized code, developed using Igor Pro data analysis software [26], was used to construct a new heat flow curve by applying a single randomly assigned error to each data point; the error was selected from within the bounds of a uniform (-a, a) distribution with

$$a = u(HF_{record}) \cdot \sqrt{3} \quad . \tag{14}$$

To simulate baseline variability, endpoints defining the peak's start and stop were randomly selected from defined intervals that varied depending on heating rate. These endpoints were

then used to construct a linear baseline for the simulated heat flow curve, the peak was integrated, and a new ΔH_{meas} was calculated. This process was repeated 10,000 times and the overall mean and standard deviation determined, with the standard deviation representing the uncertainty in the integrated peak area, $u(x)$. Figure 9 shows a sample histogram displaying the results of the enthalpy simulations for a single replicate measurement of the A1 sample at 3 °C·min^{-1}. In this example, the estimated uncertainty in the measured peak area ($u(x)$) was 0.583 mW·s. A separate determination of $u(x)$ was made for each replicate measurement, at each heating rate, for all fifteen SRM indium samples.

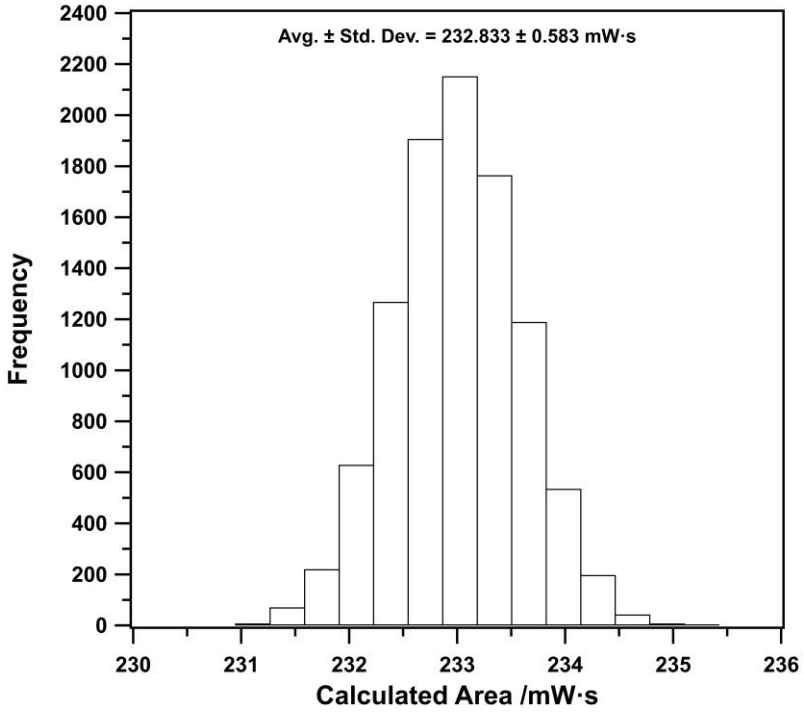

Figure 9. Sample histogram for enthalpy simulations. What is shown are the results for a single replicate measurement of the A1 sample at 3 °C·min^{-1}. The resulting average and associated standard deviation are displayed. The estimated uncertainty in the measured peak area, $u(x)$, was set equal to the standard deviation.

4.2.2. Uncertainty in Sample Mass ($u(m)$)

We have estimated the standard uncertainty in sample mass, $u(m)$, as

$$u(m) = \sqrt{u_A^2 + u_B^2}\,, \tag{15}$$

where u_A denotes a type A uncertainty evaluation and u_B denotes a type B uncertainty evaluation [25, 27]. In this work,

$$u_A = \frac{s_p}{\sqrt{n}}, \tag{16}$$

where s_p is the standard deviation of the measurement process (mg), which was determined from a balance control chart, and n is the number of replicate sample weighings [12]. The value of u_B was estimated as

$$u_B = \sqrt{u_r^2 + u_{buoy}^2 + u_s^2}\,. \tag{17}$$

The first term, u_r, is the combined standard uncertainty of all reference masses utilized in the ABBA weighing scheme (mg), which are combined as a simple sum [28]. The second term, u_{buoy}, is the uncertainty associated with the applied air buoyancy correction (mg), which was estimated as

$$u_{buoy} = \sqrt{(V_x - V_r)^2 \cdot u_{\rho_{air}}^2 + \rho_{air}^2 \cdot \left(u_{V_x} - u_{V_r}\right)^2}\,. \tag{18}$$

Here, V_x and V_r are the volumes of the sample and reference pans, respectively, and u_{V_x} and u_{V_r} are the corresponding standard uncertainties in the pan volumes. The two remaining terms refer to the calculated air density (ρ_{air}) and its standard uncertainty ($u_{\rho_{air}}$). In this work, the standard uncertainties in sample and reference pan volumes are equivalent, reducing Eq. (18) to a function of pan volumes and the uncertainty in air density. The uncertainty in calculated air density is calculated as

$$u_{\rho_{air}} = \rho_{air} \cdot \sqrt{u_T^2 + u_{RH}^2 + u_p^2 + u_{eq}^2}\,, \tag{19}$$

where u_T, u_{RH}, u_p, and u_{eq} are the relative standard uncertainties associated with the measurements of room temperature, relative humidity, and pressure, as well as the equation used in the air density calculation [29].

The final term in Eq. (17), u_s, is the uncertainty arising from balance sensitivity (mg), which was estimated using an average of individual sensitivity values determined as part of the employed

weighing scheme [12]. In this work, $u(m)$ was estimated to be 0.003 mg for all measured samples. The values for each of the primary uncertainty components are summarized in Table 8.

Table 8. Estimated Uncertainty in Sample Mass.

Component	$\boldsymbol{u(z)^a}$ **(mg)**
u_A	0.001076
u_r	0.000750
u_{buoy}	0.000004
u_s	0.002311
u_B	0.002429
$u(m)^b$	0.003

[a]Standard (k = 1) uncertainty estimate for the corresponding component.
[b]Combined standard uncertainty in sample mass calculated using Eq. (15).

5. Conclusions

The evaluation of SRM 2232a has shown that the material is of high purity (≥ 99.99999%) and is suitable for use as a temperature and enthalpy calibration standard for DSCs. A fixed-point cell constructed from SRM 2232a indium, combined with comparisons to NIST's primary realization of the indium freezing point, yielded a certified melting temperature of (156.5985 ± 0.0003) °C. The enthalpy of fusion was certified as (28.58 ± 0.17) $J \cdot g^{-1}$ via DSC measurements of 15 samples taken from seven randomly selected ingots of SRM 2232a. The DSC employed in this work was calibrated for temperature and enthalpy using certified reference materials obtained from PTB. The PTB reference materials were certified via comparison with a fixed-point standard and measurements using a modified Tian-Calvet calorimeter for temperature and enthalpy, respectively [7, 8].

References

[1] Rosasco GJ, Whetstone JR, Watters RL (2005) Certificate of Analysis - Standard Reference Material 2232 (National Institute of Standards and Technology, Gaithersburg, MD).
[2] Preston-Thomas H (1990) The International Temperature Scale of 1990 (ITS-90). *Metrologia* 27:3-10.
[3] Preston-Thomas H (1990) Erratum: The International Temperature Scale of 1990 (ITS-90). *Metrologia* 27:107.
[4] Furukawa GT, Riddle JL, Bigge WR, Pfeiffer ER (1982) Application of Some Metal SRMs as Thermometric Fixed Points (National Bureau of Standards, Gaithersburg, MD, USA), NBS SP260-77.
[5] Strouse GF (2008) Standard Platinum Resistance Thermometer Calibrations from the Ar TP to the Ag FP (National Institute of Standards and Technology, Gaithersburg, MD), NIST SP250-81.
[6] Mangum BW, Furukawa GT (1990) Guidelines for Realizing the International Temperature Scale of 1990 (ITS-90) (National Institute of Science and Technology, Gaithersburg, MD), NIST TN 1265.
[7] Sarge S, Hansen D (2018) Calibration Certificate - Indium Certified Reference Material (Physikalisch-Technische Bundesanstalt, Braunschweig, Germany).
[8] Sarge S, Hansen D (2018) Calibration Certificate - Tin Certified Reference Material (Physikalisch-Technische Bundesanstalt, Braunschweig, Germany).
[9] Boerio-Goates J, Callanan JE (1992) Differential Thermal Methods. *Physical Methods of Chemistry, Volume VI: Determination of Thermodynamic Properties*, eds Rossiter BW & Baetzold RC (John Wiley & Sons, New York, NY), Chapter 8, 2nd Ed., pp 621-717.
[10] Gmelin E, Sarge SM (1995) Calibration of Differential Scanning Calorimeters. *Pure Appl Chem* 67:1789-1800.
[11] Höhne GWH, Hemminger W, Flammersheim HJ (1996) *Differential Scanning Calorimetry: An Introduction for Practitioners* (Springer-Verlag, Berlin, Germany).
[12] Harris GL (2019) Selected Laboratory and Measurement Practices and Procedures to Support Basic Mass Calibrations (National Institute of Standards and Technology, Gaithersburg, MD), NISTIR 6969.
[13] Fortin TJ, Bruno TJ, Lovestead TM (2023) Comparison of Heat Capacity Measurements of Alternative and Conventional Aviation Fuels. *Int J Thermophys* 44:5.
[14] Della Gatta G, Richardson MJ, Sarge SM, Stølen S (2006) Standards, Calibration, and Guidelines in Microcalorimetry Part 2. Calibration Standards for Differential Scanning Calorimetry. *Pure Appl Chem* 78:1455-1476.
[15] Sarge SM, Gmelin E, Höhne GWH, Cammenga HK, Hemminger W, Eysel W (1994) The Caloric Calibration of Scanning Calorimeters. *Thermochim Acta* 247:129-168.
[16] ASTM International (2018) Standard Test Method for Temperature Calibration of Differential Scanning Calorimeters and Differential Thermal Analyzers (ASTM International, West Conshohocken, PA), ASTM E967-18.
[17] Fellmuth B, Hill KD, Pearce JV, Peruzzi A, Steur PPM, Zhang J (2018) Guide to the Realization of the ITS-90 Part 2.1 - Fixed Points: Influence of Impurities (International

Bureau of Weights and Measures (BIPM), Consultative Committee for Thermometry (CCT), Sèvres, France).
[18] Gelman A, Carlin JB, Stern HS, Dunson DB, Vehtari A, Rubin DB (2014) *Bayesian Data Analysis* (CRC Press, Boca Raton, FL), 3rd Ed.
[19] Stan Development Team (2022) Stan Modeling Language Users Guide and Reference Manual, 2.32. https://mc-stan.org
[20] R Core Team (2023) R: A Language and Environment for Statistical Computing (R Foundation for Statistical Computing, Vienna, Austria). https://www.R-project.org
[21] Stan Development Team (2022) RStan: The R Interface to Stan, 2.21.7. https://mc-stan.org
[22] Holcombe G (2021) Certificate of Measurement - Indium Certified Reference Material LGC2601 (LGC Group, Teddington, Middlesex, UK).
[23] Archer DG, Rudtsch S (2003) Enthalpy of Fusion of Indium: A Certified Reference Material for Differential Scanning Calorimetry. *J Chem Eng Data* 48:1157-1163.
[24] Stølen S, Grønvold F (1999) Critical Assessment of the Enthalpy of Fusion of Metals Used as Enthalpy Standards at Moderate to High Temperatures. *Thermochim Acta* 327:1-32.
[25] BIPM (2008) Evaluation of Measurement Data - Guide to the Expression of Uncertainty in Measurement (International Bureau of Weights and Measures (BIPM), Joint Committee for Guides in Metrology (JCGM), Sèvres, France), JCGM 100:2008.
[26] Igor Pro Development Team (2022) Igor Pro (WaveMetrics Inc., Lake Oswego, OR), 8.04. https://wavemetrics.com
[27] Kochsiek M, Gläser M (1999) *Comprehensive Mass Metrology* (Wiley-VCH, Berlin, Germany).
[28] Schwartz R (2000) Mass Determination with Balances. *Comprehensive Mass Metrology*, eds Kochsiek M & Gläser M (Wiley-VCH, Berlin, Germany), Chapter 3.4, pp 232-295.
[29] Picard A, Davis RS, Gläser M, Fujii K (2008) Revised Formula for the Density of Moist Air (CIPM-2007). *Metrologia* 45:149-155.

Appendix A. Supplemental Materials

A.1. Sample Purity Analysis

The supplier provided two certificates showing the GDMS analysis results of the high-purity indium used for SRM 2232a. Figure A.1.1 shows results from the supplier's own analysis, while the Fig. A.1.2 shows results from the analysis by an independent lab (EAG Laboratories, Shanghai, China). Units for measured impurities are parts per million (ppm) (i.e., $\mu g \cdot g^{-1}$).

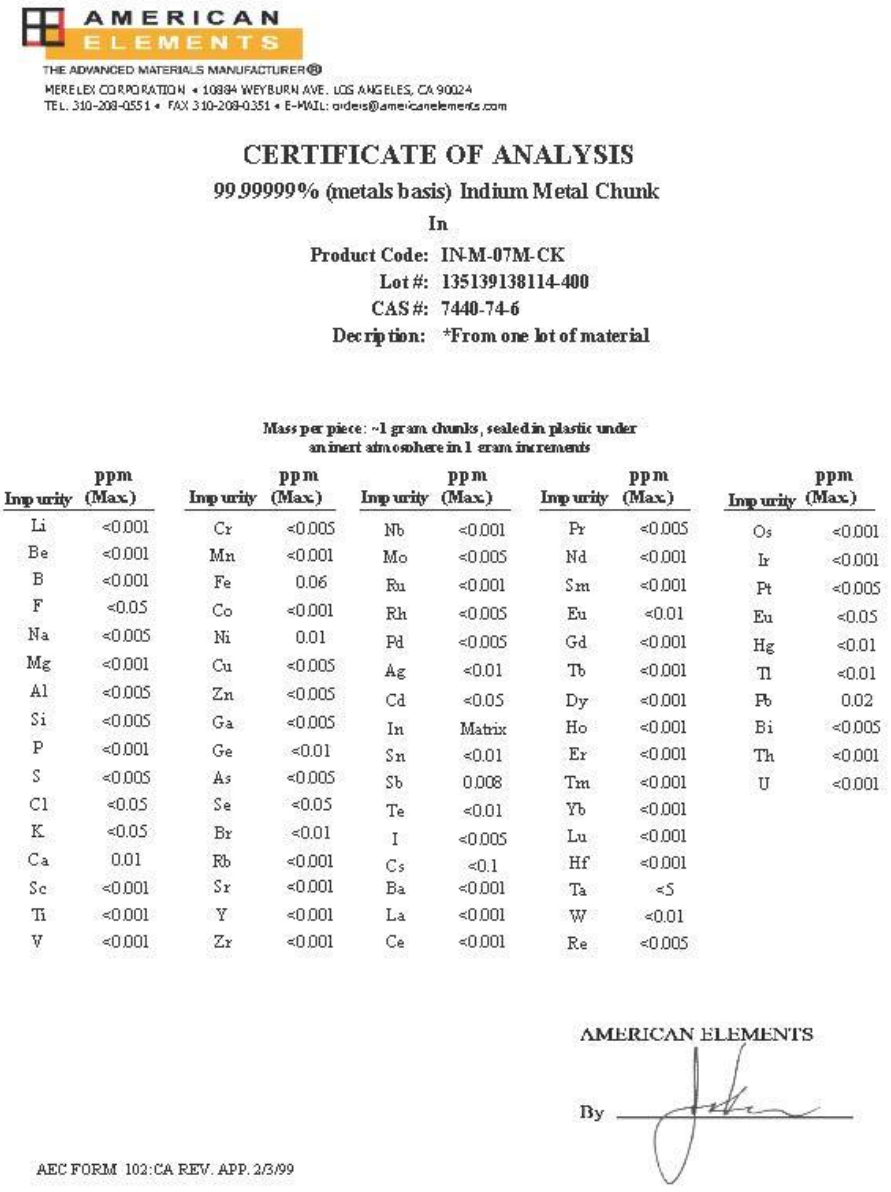

AMERICAN ELEMENTS
THE ADVANCED MATERIALS MANUFACTURER®
MERELEX CORPORATION • 10884 WEYBURN AVE. LOS ANGELES, CA 90024
TEL. 310-208-0551 • FAX 310-208-0351 • E-MAIL: orders@americanelements.com

CERTIFICATE OF ANALYSIS

99.99999% (metals basis) Indium Metal Chunk
In

Product Code: IN-M-07M-CK
Lot #: 135139138114-400
CAS #: 7440-74-6
Decription: *From one lot of material

Mass per piece: ~1 gram chunks, sealed in plastic under an inert atmosphere in 1 gram increments

Impurity	ppm (Max.)	Impurity	ppm (Max.)	Impurity	ppm (Max.)	Impurity	ppm (Max.)	Impurity	ppm (Max.)
Li	<0.001	Cr	<0.005	Nb	<0.001	Pr	<0.005	Os	<0.001
Be	<0.001	Mn	<0.001	Mo	<0.005	Nd	<0.001	Ir	<0.001
B	<0.001	Fe	0.06	Ru	<0.001	Sm	<0.001	Pt	<0.005
F	<0.05	Co	<0.001	Rh	<0.005	Eu	<0.01	Eu	<0.05
Na	<0.005	Ni	0.01	Pd	<0.005	Gd	<0.001	Hg	<0.01
Mg	<0.001	Cu	<0.005	Ag	<0.01	Tb	<0.001	Tl	<0.01
Al	<0.005	Zn	<0.005	Cd	<0.05	Dy	<0.001	Pb	0.02
Si	<0.005	Ga	<0.005	In	Matrix	Ho	<0.001	Bi	<0.005
P	<0.001	Ge	<0.01	Sn	<0.01	Er	<0.001	Th	<0.001
S	<0.005	As	<0.005	Sb	0.008	Tm	<0.001	U	<0.001
Cl	<0.05	Se	<0.05	Te	<0.01	Yb	<0.001		
K	<0.05	Br	<0.01	I	<0.005	Lu	<0.001		
Ca	0.01	Rb	<0.001	Cs	<0.1	Hf	<0.001		
Sc	<0.001	Sr	<0.001	Ba	<0.001	Ta	<5		
Ti	<0.001	Y	<0.001	La	<0.001	W	<0.01		
V	<0.001	Zr	<0.001	Ce	<0.001	Re	<0.005		

AMERICAN ELEMENTS
By

AEC FORM 102:CA REV. APP. 2/3/99

Figure A.1.1. Certificate of analysis provided by supplier.

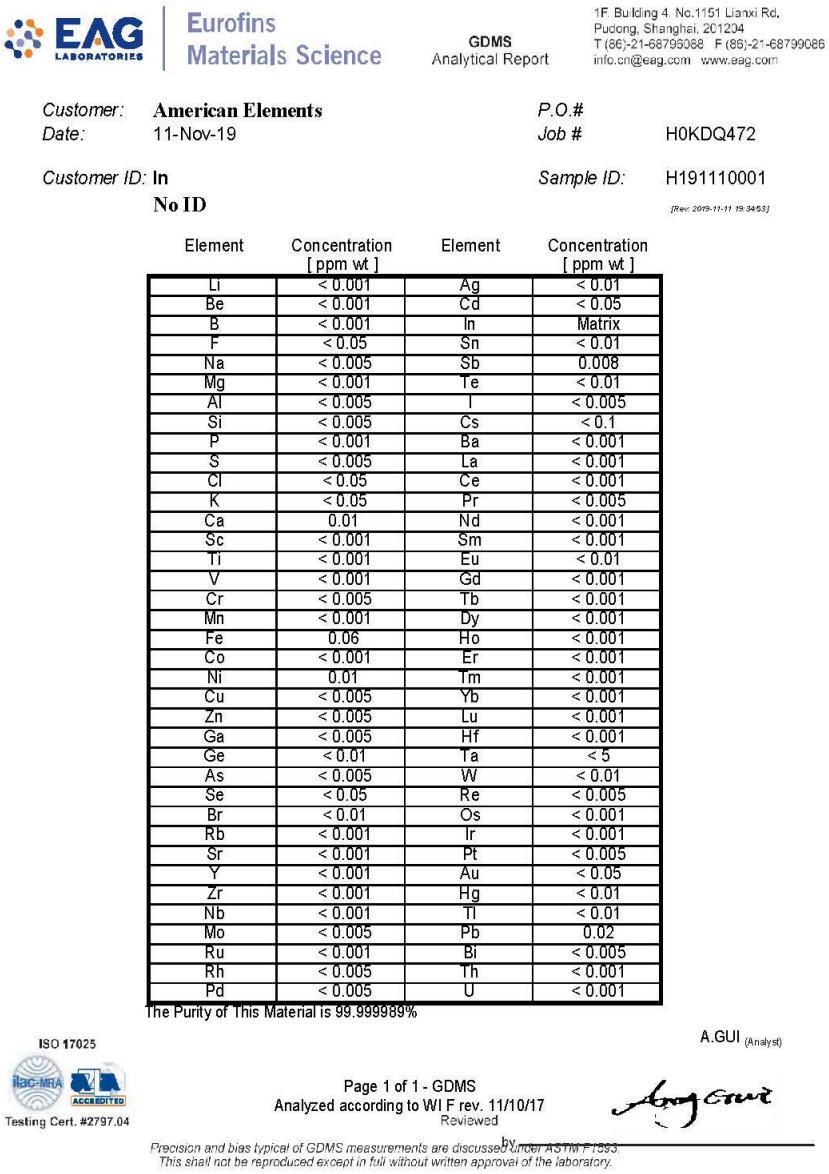

EAG LABORATORIES | Eurofins Materials Science

GDMS
Analytical Report

1F, Building 4, No.1151 Lianxi Rd,
Pudong, Shanghai, 201204
T (86)-21-68799088 F (86)-21-68799086
info.cn@eag.com www.eag.com

Customer: **American Elements** *P.O.#*
Date: 11-Nov-19 *Job #* H0KDQ472

Customer ID: In *Sample ID:* H191110001
No ID

[Rev: 2019-11-11 19:34:53]

Element	Concentration [ppm wt]	Element	Concentration [ppm wt]
Li	< 0.001	Ag	< 0.01
Be	< 0.001	Cd	< 0.05
B	< 0.001	In	Matrix
F	< 0.05	Sn	< 0.01
Na	< 0.005	Sb	0.008
Mg	< 0.001	Te	< 0.01
Al	< 0.005	I	< 0.005
Si	< 0.005	Cs	< 0.1
P	< 0.001	Ba	< 0.001
S	< 0.005	La	< 0.001
Cl	< 0.05	Ce	< 0.001
K	< 0.05	Pr	< 0.005
Ca	0.01	Nd	< 0.001
Sc	< 0.001	Sm	< 0.001
Ti	< 0.001	Eu	< 0.01
V	< 0.001	Gd	< 0.001
Cr	< 0.005	Tb	< 0.001
Mn	< 0.001	Dy	< 0.001
Fe	0.06	Ho	< 0.001
Co	< 0.001	Er	< 0.001
Ni	0.01	Tm	< 0.001
Cu	< 0.005	Yb	< 0.001
Zn	< 0.005	Lu	< 0.001
Ga	< 0.005	Hf	< 0.001
Ge	< 0.01	Ta	< 5
As	< 0.005	W	< 0.01
Se	< 0.05	Re	< 0.005
Br	< 0.01	Os	< 0.001
Rb	< 0.001	Ir	< 0.001
Sr	< 0.001	Pt	< 0.005
Y	< 0.001	Au	< 0.05
Zr	< 0.001	Hg	< 0.01
Nb	< 0.001	Tl	< 0.01
Mo	< 0.005	Pb	0.02
Ru	< 0.001	Bi	< 0.005
Rh	< 0.005	Th	< 0.001
Pd	< 0.005	U	< 0.001

The Purity of This Material is 99.999989%

ISO 17025

Testing Cert. #2797.04

A.GUI (Analyst)

Page 1 of 1 - GDMS
Analyzed according to WI F rev. 11/10/17
Reviewed

by

Precision and bias typical of GDMS measurements are discussed under ASTM F1393.

Figure A.1.2. Results of independent analysis provided by supplier.

To verify the analysis results provided by the supplier, and test for lot homogeneity, we sent six samples to NRC Canada for GDMS analysis. The samples were taken from six of the seven ingots used in the enthalpy of fusion measurements (labelled “A” – “F”). The certificates are shown in Figs. A.1.3 – A.1.8. Units for measured impurities are parts per billion (ppb), where 1 ppb = 0.001 $\mu g \cdot g^{-1}$. The results indicate sample purities of 99.9999996% (samples A, E, and F) and 99.9999997% (samples B, C, and D), which are consistent with the purity information provided

by the supplier. Additionally, no statistically significant difference was observed between the samples, indicating lot homogeneity.

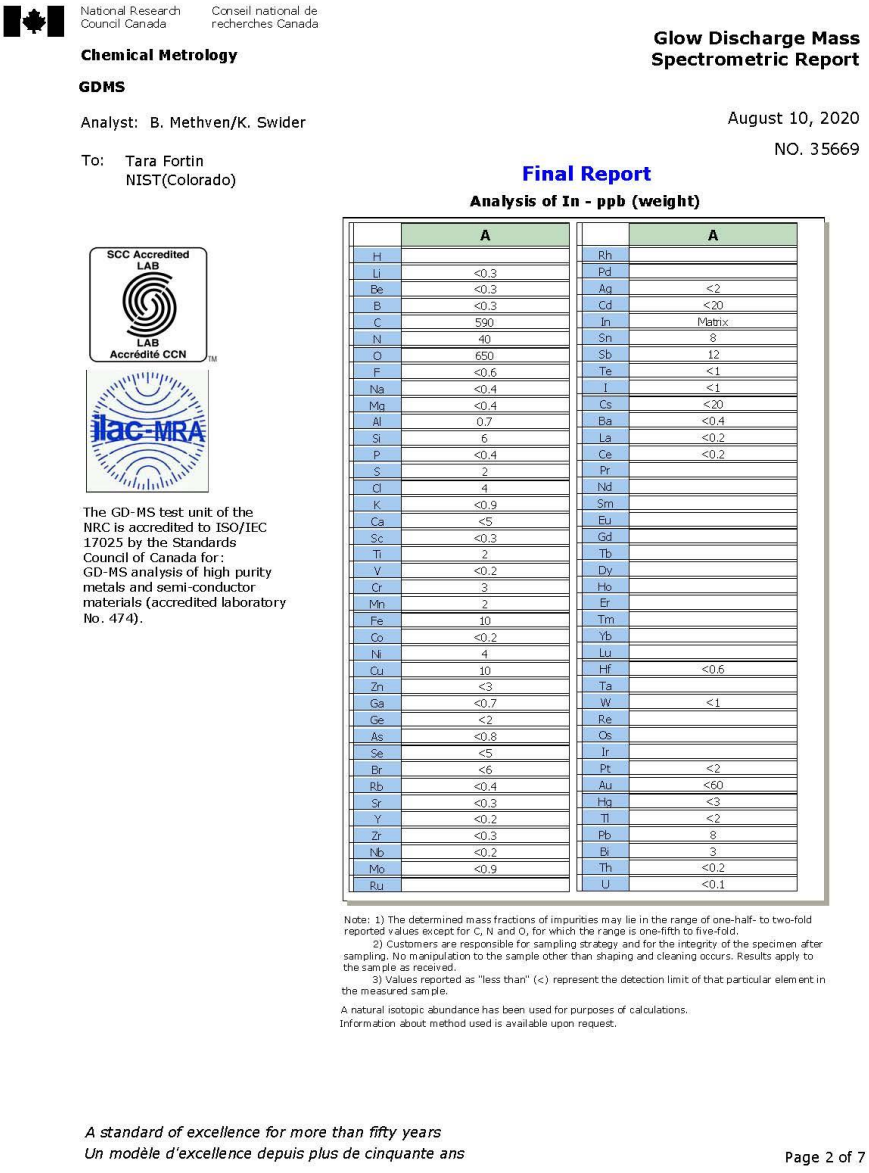

National Research Council Canada / Conseil national de recherches Canada

Chemical Metrology

GDMS

Analyst: B. Methven/K. Swider

To: Tara Fortin
NIST(Colorado)

Glow Discharge Mass Spectrometric Report

August 10, 2020

NO. 35669

Final Report

Analysis of In - ppb (weight)

	A		A
H		Rh	
Li	<0.3	Pd	
Be	<0.3	Ag	<2
B	<0.3	Cd	<20
C	590	In	Matrix
N	40	Sn	8
O	650	Sb	12
F	<0.6	Te	<1
Na	<0.4	I	<1
Mg	<0.4	Cs	<20
Al	0.7	Ba	<0.4
Si	6	La	<0.2
P	<0.4	Ce	<0.2
S	2	Pr	
Cl	4	Nd	
K	<0.9	Sm	
Ca	<5	Eu	
Sc	<0.3	Gd	
Ti	2	Tb	
V	<0.2	Dy	
Cr	3	Ho	
Mn	2	Er	
Fe	10	Tm	
Co	<0.2	Yb	
Ni	4	Lu	
Cu	10	Hf	<0.6
Zn	<3	Ta	
Ga	<0.7	W	<1
Ge	<2	Re	
As	<0.8	Os	
Se	<5	Ir	
Br	<6	Pt	<2
Rb	<0.4	Au	<60
Sr	<0.3	Hg	<3
Y	<0.2	Tl	<2
Zr	<0.3	Pb	8
Nb	<0.2	Bi	3
Mo	<0.9	Th	<0.2
Ru		U	<0.1

SCC Accredited LAB
LAB Accrédité CCN

ilac-MRA

The GD-MS test unit of the NRC is accredited to ISO/IEC 17025 by the Standards Council of Canada for: GD-MS analysis of high purity metals and semi-conductor materials (accredited laboratory No. 474).

Note: 1) The determined mass fractions of impurities may lie in the range of one-half- to two-fold reported values except for C, N and O, for which the range is one-fifth to five-fold.
2) Customers are responsible for sampling strategy and for the integrity of the specimen after sampling. No manipulation to the sample other than shaping and cleaning occurs. Results apply to the sample as received.
3) Values reported as "less than" (<) represent the detection limit of that particular element in the measured sample.

A natural isotopic abundance has been used for purposes of calculations.
Information about method used is available upon request.

A standard of excellence for more than fifty years
Un modèle d'excellence depuis plus de cinquante ans

Page 2 of 7

Figure A.1.3. Analysis report for sample A provided by NRC Canada.

National Research Council Canada | Conseil national de recherches Canada

Chemical Metrology

GDMS

Glow Discharge Mass Spectrometric Report

Analyst: B. Methven/K. Swider

August 10, 2020

NO. 35669

To: Tara Fortin
NIST(Colorado)

Final Report

Analysis of In - ppb (weight)

	B		B
H		Rh	
Li	<0.3	Pd	
Be	<0.3	Ag	<2
B	<0.3	Cd	<20
C	420	In	Matrix
N	40	Sn	12
O	350	Sb	9
F	<1	Te	<1
Na	<0.5	I	<0.9
Mg	<0.4	Cs	<15
Al	4	Ba	<0.4
Si	2	La	<0.2
P	<0.5	Ce	<0.2
S	0.6	Pr	
Cl	4	Nd	
K	<0.7	Sm	
Ca	<6	Eu	
Sc	<0.3	Gd	
Ti	0.7	Tb	
V	<0.2	Dy	
Cr	<0.5	Ho	
Mn	<0.5	Er	
Fe	9	Tm	
Co	<0.2	Yb	
Ni	6	Lu	
Cu	<1	Hf	<0.7
Zn	<4	Ta	
Ga	<0.6	W	<1
Ge	<3	Re	
As	<1	Os	
Se	<9	Ir	
Br	<5	Pt	<2
Rb	<0.4	Au	<45
Sr	<0.3	Hg	<4
Y	<0.2	Tl	<4
Zr	<0.3	Pb	10
Nb	<0.3	Bi	4
Mo	<1	Th	<0.2
Ru		U	<0.2

SCC Accredited LAB
LAB Accrédité CCN

ilac-MRA

The GD-MS test unit of the NRC is accredited to ISO/IEC 17025 by the Standards Council of Canada for: GD-MS analysis of high purity metals and semi-conductor materials (accredited laboratory No. 474).

Note: 1) The determined mass fractions of impurities may lie in the range of one-half- to two-fold reported values except for C, N and O, for which the range is one-fifth to five-fold.
2) Customers are responsible for sampling strategy and for the integrity of the specimen after sampling. No manipulation to the sample other than shaping and cleaning occurs. Results apply to the sample as received.
3) Values reported as "less than" (<) represent the detection limit of that particular element in the measured sample.

A natural isotopic abundance has been used for purposes of calculations.
Information about method used is available upon request.

A standard of excellence for more than fifty years
Un modèle d'excellence depuis plus de cinquante ans

Page 3 of 7

Figure A.1.4. Analysis report for sample B provided by NRC Canada.

National Research Council Canada | Conseil national de recherches Canada

Chemical Metrology

GDMS

Glow Discharge Mass Spectrometric Report

Analyst: B. Methven/K. Swider

August 10, 2020

NO. 35669

To: Tara Fortin
NIST(Colorado)

Final Report

Analysis of In - ppb (weight)

	C		C
H		Rh	
Li	<0.3	Pd	
Be	<0.3	Ag	<2
B	<0.3	Cd	<20
C	330	In	Matrix
N	20	Sn	15
O	400	Sb	6
F	<0.8	Te	<2
Na	<0.7	I	<1
Mg	<0.4	Cs	<7
Al	2	Ba	<0.4
Si	6	La	<0.2
P	<0.4	Ce	<0.2
S	2	Pr	
Cl	4	Nd	
K	<1	Sm	
Ca	<8	Eu	
Sc	<0.3	Gd	
Ti	0.5	Tb	
V	<0.2	Dy	
Cr	<0.7	Ho	
Mn	2	Er	
Fe	8	Tm	
Co	<0.3	Yb	
Ni	2	Lu	
Cu	<1	Hf	<0.6
Zn	<4	Ta	
Ga	<0.7	W	<1
Ge	<4	Re	
As	<0.8	Os	
Se	<5	Ir	
Br	<5	Pt	<2
Rb	<0.4	Au	<45
Sr	<0.3	Hg	<4
Y	<0.2	Tl	<2
Zr	<0.3	Pb	11
Nb	<0.3	Bi	5
Mo	<1	Th	<0.2
Ru		U	<0.2

SCC Accredited LAB
LAB Accrédité CCN

ilac-MRA

The GD-MS test unit of the NRC is accredited to ISO/IEC 17025 by the Standards Council of Canada for: GD-MS analysis of high purity metals and semi-conductor materials (accredited laboratory No. 474).

Note: 1) The determined mass fractions of impurities may lie in the range of one-half- to two-fold reported values except for C, N and O, for which the range is one-fifth to five-fold.
2) Customers are responsible for sampling strategy and for the integrity of the specimen after sampling. No manipulation to the sample other than shaping and cleaning occurs. Results apply to the sample as received.
3) Values reported as "less than" (<) represent the detection limit of that particular element in the measured sample.

A natural isotopic abundance has been used for purposes of calculations.
Information about method used is available upon request.

A standard of excellence for more than fifty years
Un modèle d'excellence depuis plus de cinquante ans

Page 4 of 7

Figure A.1.5. Analysis report for sample C provided by NRC Canada.

National Research Council Canada | Conseil national de recherches Canada

Chemical Metrology

GDMS

Glow Discharge Mass Spectrometric Report

Analyst: B. Methven/K. Swider

August 10, 2020

NO. 35669

To: Tara Fortin
NIST(Colorado)

Final Report

Analysis of In - ppb (weight)

	D		D
H		Rh	
Li	<0.3	Pd	
Be	<0.3	Ag	<2
B	<0.3	Cd	<20
C	340	In	Matrix
N	25	Sn	8
O	410	Sb	4
F	<0.9	Te	<1
Na	<0.5	I	<1
Mg	<0.5	Cs	<10
Al	4	Ba	<0.4
Si	16	La	<0.2
P	<0.6	Ce	<0.3
S	1	Pr	
Cl	3	Nd	
K	<0.9	Sm	
Ca	<6	Eu	
Sc	<0.2	Gd	
Ti	1	Tb	
V	<0.2	Dy	
Cr	<0.6	Ho	
Mn	2	Er	
Fe	6	Tm	
Co	<0.2	Yb	
Ni	2	Lu	
Cu	<1	Hf	<0.7
Zn	<3	Ta	
Ga	<0.6	W	<1
Ge	<3	Re	
As	<0.8	Os	
Se	<5	Ir	
Br	<4	Pt	<2
Rb	<0.4	Au	<40
Sr	<0.3	Hg	<4
Y	<0.3	Tl	<2
Zr	<0.6	Pb	13
Nb	<0.2	Bi	1
Mo	<1	Th	<0.2
Ru		U	<0.2

SCC Accredited LAB
LAB Accrédité CCN

ilac-MRA

The GD-MS test unit of the NRC is accredited to ISO/IEC 17025 by the Standards Council of Canada for: GD-MS analysis of high purity metals and semi-conductor materials (accredited laboratory No. 474).

Note: 1) The determined mass fractions of impurities may lie in the range of one-half- to two-fold reported values except for C, N and O, for which the range is one-fifth to five-fold.
2) Customers are responsible for sampling strategy and for the integrity of the specimen after sampling. No manipulation to the sample other than shaping and cleaning occurs. Results apply to the sample as received.
3) Values reported as "less than" (<) represent the detection limit of that particular element in the measured sample.

A natural isotopic abundance has been used for purposes of calculations.
Information about method used is available upon request.

A standard of excellence for more than fifty years
Un modèle d'excellence depuis plus de cinquante ans

Page 5 of 7

Figure A.1.6. Analysis report for sample D provided by NRC Canada.

National Research Council Canada | Conseil national de recherches Canada

Chemical Metrology

GDMS

Glow Discharge Mass Spectrometric Report

Analyst: B. Methven/K. Swider

August 10, 2020

NO. 35669

To: Tara Fortin
NIST(Colorado)

Final Report

Analysis of In - ppb (weight)

	E		E
H		Rh	
Li	<0.4	Pd	
Be	<0.4	Ag	<3
B	<0.4	Cd	<25
C	450	In	Matrix
N	25	Sn	9
O	620	Sb	7
F	<1	Te	<2
Na	<0.6	I	<2
Mg	<0.5	Cs	<20
Al	<0.3	Ba	<0.5
Si	4	La	<0.2
P	<0.6	Ce	<0.4
S	0.8	Pr	
Cl	5	Nd	
K	<1	Sm	
Ca	<7	Eu	
Sc	<0.4	Gd	
Ti	1	Tb	
V	<0.3	Dy	
Cr	2	Ho	
Mn	2	Er	
Fe	8	Tm	
Co	<0.2	Yb	
Ni	3	Lu	
Cu	10	Hf	<0.8
Zn	<3	Ta	
Ga	<0.9	W	<1
Ge	<3	Re	
As	<1	Os	
Se	<5	Ir	
Br	<9	Pt	<3
Rb	<0.6	Au	<60
Sr	<0.4	Hg	<5
Y	<0.4	Tl	<2
Zr	<0.4	Pb	6
Nb	<0.3	Bi	2
Mo	<1	Th	<0.3
Ru		U	<0.3

SCC Accredited LAB
LAB Accrédité CCN

ilac-MRA

The GD-MS test unit of the NRC is accredited to ISO/IEC 17025 by the Standards Council of Canada for: GD-MS analysis of high purity metals and semi-conductor materials (accredited laboratory No. 474).

Note: 1) The determined mass fractions of impurities may lie in the range of one-half- to two-fold reported values except for C, N and O, for which the range is one-fifth to five-fold.
2) Customers are responsible for sampling strategy and for the integrity of the specimen after sampling. No manipulation to the sample other than shaping and cleaning occurs. Results apply to the sample as received.
3) Values reported as "less than" (<) represent the detection limit of that particular element in the measured sample.

A natural isotopic abundance has been used for purposes of calculations.
Information about method used is available upon request.

A standard of excellence for more than fifty years
Un modèle d'excellence depuis plus de cinquante ans

Page 6 of 7

Figure A.1.7. Analysis report for sample E provided by NRC Canada.

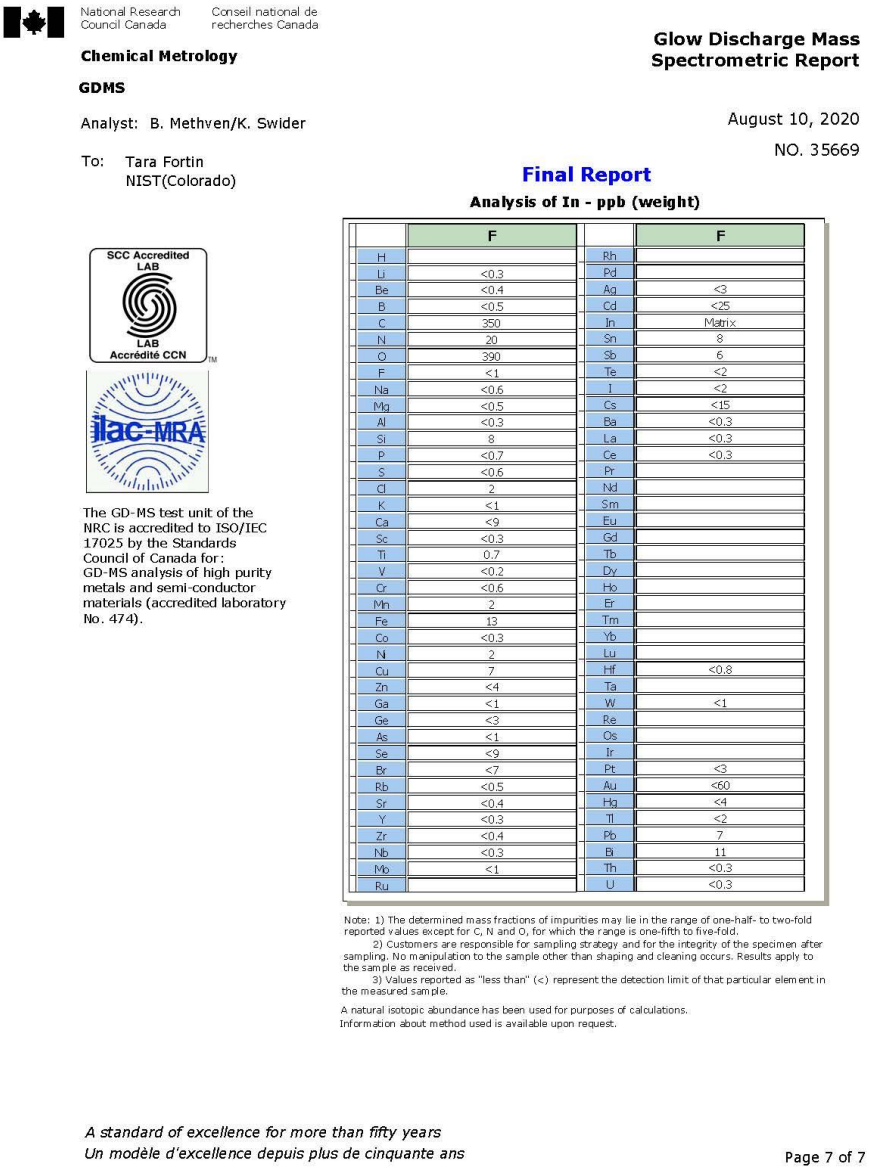

National Research Council Canada / Conseil national de recherches Canada

Chemical Metrology

GDMS

Analyst: B. Methven/K. Swider

To: Tara Fortin
NIST(Colorado)

Glow Discharge Mass Spectrometric Report

August 10, 2020

NO. 35669

Final Report

Analysis of In - ppb (weight)

	F		F
H		Rh	
Li	<0.3	Pd	
Be	<0.4	Ag	<3
B	<0.5	Cd	<25
C	350	In	Matrix
N	20	Sn	8
O	390	Sb	6
F	<1	Te	<2
Na	<0.6	I	<2
Mg	<0.5	Cs	<15
Al	<0.3	Ba	<0.3
Si	8	La	<0.3
P	<0.7	Ce	<0.3
S	<0.6	Pr	
Cl	2	Nd	
K	<1	Sm	
Ca	<9	Eu	
Sc	<0.3	Gd	
Ti	0.7	Tb	
V	<0.2	Dy	
Cr	<0.6	Ho	
Mn	2	Er	
Fe	13	Tm	
Co	<0.3	Yb	
Ni	2	Lu	
Cu	7	Hf	<0.8
Zn	<4	Ta	
Ga	<1	W	<1
Ge	<3	Re	
As	<1	Os	
Se	<9	Ir	
Br	<7	Pt	<3
Rb	<0.5	Au	<60
Sr	<0.4	Hg	<4
Y	<0.3	Tl	<2
Zr	<0.4	Pb	7
Nb	<0.3	Bi	11
Mo	<1	Th	<0.3
Ru		U	<0.3

SCC Accredited LAB
LAB Accrédité CCN

ilac-MRA

The GD-MS test unit of the NRC is accredited to ISO/IEC 17025 by the Standards Council of Canada for: GD-MS analysis of high purity metals and semi-conductor materials (accredited laboratory No. 474).

Note: 1) The determined mass fractions of impurities may lie in the range of one-half- to two-fold reported values except for C, N and O, for which the range is one-fifth to five-fold.
2) Customers are responsible for sampling strategy and for the integrity of the specimen after sampling. No manipulation to the sample other than shaping and cleaning occurs. Results apply to the sample as received.
3) Values reported as "less than" (<) represent the detection limit of that particular element in the measured sample.

A natural isotopic abundance has been used for purposes of calculations.
Information about method used is available upon request.

A standard of excellence for more than fifty years
Un modèle d'excellence depuis plus de cinquante ans

Page 7 of 7

Figure A.1.8. Analysis report for sample F provided by NRC Canada.

A.2. Enthalpy of Fusion Measurement Results

Individual replicate enthalpy of fusion measurement results (ΔH_{meas}) for all samples are shown in Table A.2.1. Also included in the table are the corresponding sample mass, the measured heating rate (β_{avg}), and the combined standard uncertainty in enthalpy ($u(\Delta H_{meas})$). Results have been sorted by heating rate and sample mass; at each heating rate, for a given sample, results are reported in the order the measurements were made.

Table A.2.1. Replicate Enthalpy of Fusion Measurement Results for Fifteen SRM 2232a Samples at Four Heating Rates.

Sample	Mass (mg)	$\beta_{avg}{}^{a}$ (°C·min^{-1})	$\Delta H_{meas}{}^{b}$ (J·g^{-1})	$u(\Delta H_{meas})^{c}$ (J·g^{-1})
D2	7.296	1.000	28.68	0.09
D2	7.296	0.999	28.31	0.09
D2	7.296	0.999	28.54	0.09
D	7.574	0.999	27.58	0.09
D	7.574	0.999	28.82	0.09
D	7.574	0.999	28.78	0.09
A3	8.011	0.999	28.59	0.09
A3	8.011	0.999	29.00	0.09
A3	8.011	0.999	28.69	0.09
A2	8.078	0.999	28.33	0.09
A2	8.078	0.999	28.52	0.09
A2	8.078	0.999	28.66	0.09
A1	8.118	0.999	28.08	0.09
A1	8.118	0.999	28.79	0.09
A1	8.118	0.999	28.66	0.09
B1	8.146	0.999	28.53	0.09
B1	8.146	0.999	28.59	0.09
B1	8.146	0.999	28.72	0.09
A4	8.148	0.999	28.29	0.09
A4	8.148	0.999	28.25	0.09
A4	8.148	1.000	28.37	0.09
A5	8.163	0.999	28.68	0.09
A5	8.163	0.999	28.74	0.09
A5	8.163	0.999	28.79	0.09
B3	8.224	0.999	28.58	0.09
B3	8.224	0.999	28.47	0.09
B3	8.224	0.999	28.70	0.09
B2	8.233	0.999	28.65	0.09

Table A.2.1. continued.

Sample	Mass (mg)	$\beta_{avg}{}^{a}$ (°C·min^{-1})	$\Delta H_{meas}{}^{b}$ (J·g^{-1})	$u(\Delta H_{meas})^{c}$ (J·g^{-1})
B2	8.233	0.999	28.62	0.09
B2	8.233	0.999	28.73	0.09
F	9.551	0.999	28.80	0.09
F	9.551	0.999	28.59	0.09
F	9.551	0.999	28.65	0.09
E	10.647	0.999	28.77	0.09
E	10.647	0.999	28.55	0.09
E	10.647	0.999	28.56	0.09
G2	13.185	1.000	28.65	0.09
G2	13.185	1.000	28.64	0.09
G2	13.185	0.999	28.84	0.09
G	13.258	0.999	28.77	0.09
G	13.258	0.999	28.13	0.09
G	13.258	0.999	28.56	0.09
C	13.663	0.999	28.51	0.09
C	13.663	0.999	28.69	0.09
C	13.663	0.999	28.73	0.09
D2	7.296	2.999	28.44	0.07
D2	7.296	2.999	28.55	0.07
D2	7.296	2.999	28.64	0.07
D	7.574	2.999	28.64	0.07
D	7.574	2.999	28.66	0.07
D	7.574	2.999	28.70	0.07
A3	8.011	2.999	28.70	0.07
A3	8.011	2.999	28.75	0.07
A3	8.011	2.999	28.69	0.07
A2	8.078	2.999	28.76	0.07
A2	8.078	2.999	28.63	0.07
A2	8.078	2.999	28.76	0.07

Table A.2.1. continued.

Sample	Mass (mg)	$\beta_{avg}{}^{a}$ (°C·min^{-1})	$\Delta H_{meas}{}^{b}$ (J·g^{-1})	$u(\Delta H_{meas})^{c}$ (J·g^{-1})
A1	8.118	2.999	28.67	0.07
A1	8.118	2.999	28.68	0.07
A1	8.118	2.998	28.71	0.07
B1	8.146	2.999	28.92	0.07
B1	8.146	2.999	28.87	0.07
B1	8.146	2.999	28.82	0.07
A4	8.148	2.999	28.45	0.07
A4	8.148	2.998	28.32	0.07
A4	8.148	2.999	28.30	0.07
A5	8.163	2.999	28.66	0.07
A5	8.163	2.998	28.51	0.07
A5	8.163	2.998	28.68	0.07
B3	8.224	2.999	28.72	0.07
B3	8.224	2.998	28.61	0.08
B3	8.224	2.999	28.67	0.07
B2	8.233	2.999	28.65	0.07
B2	8.233	2.999	28.39	0.07
B2	8.233	2.999	28.71	0.07
F	9.551	2.999	28.69	0.07
F	9.551	2.999	28.64	0.07
F	9.551	2.999	28.66	0.07
E	10.647	2.999	28.54	0.07
E	10.647	2.999	28.65	0.07
E	10.647	2.999	28.59	0.07
G2	13.185	2.999	28.67	0.07
G2	13.185	2.999	28.72	0.07
G2	13.185	2.999	28.40	0.07
G	13.258	2.999	28.81	0.07
G	13.258	2.999	28.74	0.07
G	13.258	2.999	28.81	0.07

Table A.2.1. continued.

Sample	Mass (mg)	$\beta_{avg}{}^{a}$ (°C·min^{-1})	$\Delta H_{meas}{}^{b}$ (J·g^{-1})	$u(\Delta H_{meas})^{c}$ (J·g^{-1})
C	13.663	2.999	28.75	0.07
C	13.663	2.999	28.88	0.07
C	13.663	2.999	28.55	0.07
D2	7.296	4.998	28.76	0.10
D2	7.296	4.998	28.73	0.11
D2	7.296	4.998	28.40	0.11
D	7.574	4.998	28.77	0.11
D	7.574	4.998	28.70	0.11
D	7.574	4.998	28.69	0.11
A3	8.011	4.998	28.89	0.11
A3	8.011	4.998	28.90	0.11
A3	8.011	4.998	28.92	0.11
A2	8.078	4.998	28.87	0.11
A2	8.078	4.998	28.92	0.11
A2	8.078	4.998	28.78	0.11
A1	8.118	4.998	28.77	0.11
A1	8.118	4.998	28.77	0.11
A1	8.118	4.998	28.71	0.11
B1	8.146	4.998	28.86	0.11
B1	8.146	4.998	28.82	0.11
B1	8.146	4.998	28.97	0.11
A4	8.148	4.998	28.25	0.11
A4	8.148	4.998	28.18	0.11
A4	8.148	4.998	28.14	0.10
A5	8.163	4.998	28.68	0.10
A5	8.163	4.998	28.70	0.10
A5	8.163	4.998	28.52	0.10
B3	8.224	4.998	28.69	0.10
B3	8.224	4.998	28.78	0.10

Table A.2.1. continued.

Sample	Mass (mg)	β_{avg}[a] (°C·min^{-1})	ΔH_{meas}[b] (J·g^{-1})	$u(\Delta H_{meas})$[c] (J·g^{-1})
B3	8.224	4.998	28.82	0.10
B2	8.233	4.998	28.78	0.10
B2	8.233	4.998	28.79	0.10
B2	8.233	4.998	28.72	0.10
F	9.551	4.998	28.69	0.10
F	9.551	4.998	28.66	0.10
F	9.551	4.998	28.73	0.10
E	10.647	4.998	28.77	0.10
E	10.647	4.998	28.53	0.10
E	10.647	4.998	28.77	0.10
G2	13.185	4.998	28.45	0.10
G2	13.185	4.998	28.48	0.10
G2	13.185	4.998	28.26	0.10
G	13.258	4.998	28.87	0.11
G	13.258	4.998	28.83	0.11
G	13.258	4.998	28.80	0.11
C	13.663	4.998	28.89	0.11
C	13.663	4.998	28.83	0.11
C	13.663	4.998	28.90	0.11
D2	7.296	9.999	28.81	0.19
D2	7.296	9.998	28.76	0.19
D2	7.296	9.998	28.69	0.19
D	7.574	9.998	28.90	0.19
D	7.574	9.997	28.82	0.19
D	7.574	9.997	28.91	0.19
A3	8.011	9.998	28.95	0.19
A3	8.011	9.998	28.97	0.19
A3	8.011	9.998	28.95	0.19
A2	8.078	9.998	28.79	0.19

Table A.2.1. continued.

Sample	Mass (mg)	$\beta_{avg}{}^{a}$ (°C·min^{-1})	$\Delta H_{meas}{}^{b}$ (J·g^{-1})	$u(\Delta H_{meas})^{c}$ (J·g^{-1})
A2	8.078	9.998	28.87	0.19
A2	8.078	9.998	28.93	0.19
A1	8.118	9.997	28.89	0.19
A1	8.118	9.997	28.97	0.19
A1	8.118	9.998	28.94	0.19
B1	8.146	9.998	29.12	0.19
B1	8.146	9.998	29.06	0.19
B1	8.146	9.997	29.09	0.19
A4	8.148	9.997	28.39	0.19
A4	8.148	9.998	28.41	0.19
A4	8.148	9.998	28.40	0.19
A5	8.163	9.997	28.70	0.19
A5	8.163	9.997	28.64	0.19
A5	8.163	9.998	28.78	0.19
B3	8.224	9.998	28.79	0.19
B3	8.224	9.997	28.86	0.19
B3	8.224	9.997	28.84	0.19
B2	8.233	9.998	28.81	0.19
B2	8.233	9.998	28.83	0.19
B2	8.233	9.998	28.86	0.19
F	9.551	9.998	28.93	0.19
F	9.551	9.997	28.90	0.19
F	9.551	9.997	28.88	0.19
E	10.647	9.997	28.84	0.19
E	10.647	9.997	28.82	0.19
E	10.647	9.997	28.82	0.19
G2	13.185	9.998	28.59	0.19
G2	13.185	9.998	28.62	0.18
G2	13.185	9.997	28.42	0.18
G	13.258	9.997	28.88	0.19

Table A.2.1. continued.

Sample	Mass (mg)	$\beta_{avg}{}^{a}$ (°C·min^{-1})	$\Delta H_{meas}{}^{b}$ (J·g^{-1})	$u(\Delta H_{meas})^{c}$ (J·g^{-1})
G	13.258	9.998	28.61	0.19
G	13.258	9.997	28.87	0.19
C	13.663	9.998	28.95	0.19
C	13.663	9.998	28.92	0.19
C	13.663	9.998	28.93	0.19

[a]Measured heating rate. [b]Measured enthalpy of fusion. [c]Combined standard uncertainty.

A.3. Hierarchical Bayesian Model Posterior Predictive Checks

We performed posterior predictive checks to verify that the hierarchical Bayes model and its results discussed in Sec. 3.2 are reasonable. Specifically, we use the model and samples from the posterior to predict new values of ΔH_{meas}. In Fig. A.3.1, we compare histograms of the observed values to the predicted values. The row marked "Observed" shows the measured data; for example, the histogram on the first row under β = 1 °C·min^{-1} summarizes all measured values at that nominal heating rate.

Each histogram for the "Simulated" data summarizes a randomly generated set of 45 predicted values, matching the size of the observed samples. These predicted values are simulated by plugging posterior samples of the parameter values into the model we defined in Eq. (1). We generated five sets of these for each β value. These predicted values are depicted in rows below the corresponding true histogram; for example, rows 2 – 6 of the first column show five separate sets of samples simulated from the posterior distribution for β = 1 °C·min^{-1}. In all cases, the histograms of samples from the predicted values look reasonably similar to the observed data, indicating that the proposed model is reasonable for this data.

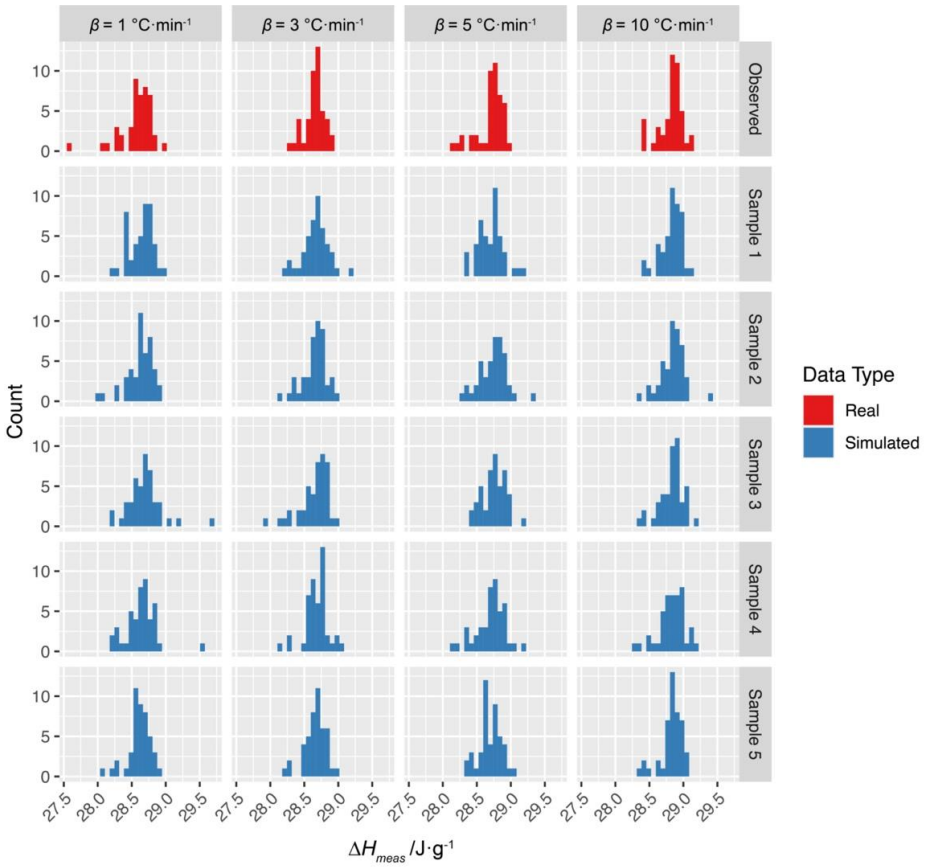

Figure A.3.1. Histogram results of posterior predictive checks. Measured enthalpies of fusion are shown in red for each of the four nominal heating rates. Simulated predicted enthalpies of fusion are shown in blue. Five separate sets of simulated samples are shown for each of the four nominal heating rates.